DEPARTMENT OF MATERIAL SCIENCE AND TECHNOLOGY
UNIVERSITY OF CRETE

Tissue Engineering - Regenerative Medicine
and Immuno-Engineering Laboratory

Institute of Electronic Structure and Laser

In vitro investigation of the cellular mechanisms activated by GO and rGO in Mesenchymal Stem Cells (MSCs)

UNDERGRADUATE THESIS

Lito - Anastasia Papadopoulou

Researcher Supervisor: Dr. Anthi Ranella

Professor Supervisor: Kelly Velonia

HERAKLION, CRETE,
2022

Acknowledgments

I would like to express my deeply gratitude to my supervisor, Dr. Anthi Ranella for giving me the opportunity to work in the laboratory of Tissue Engineering-Regenerative Medicine and Immuno-engineering (TERMIM), for all the knowledge and the experience that I obtained and her support during this thesis. Also, I would like to thank Prof. Kelly Velonia for accepting this collaboration and for being in the examination committee of my bachelor thesis.

I would like to sincerely thank Dr. Phanee Mangana for mentoring, advising and supporting me till the end of this thesis, even from hundred miles away. Her guidance and presence were invaluable, I am very grateful for having her as my mentor and I hope did not give her a hard time.

Furthermore, I am also thankful to each member of TERMIM group separately, for their help, teaching and for all the moments we have spent in the lab. It was an honor working with you all! Special thanks go to my friend and team member Maria Papada for the extremely long conversations, happy and difficult moments that we shared together.

Finally, I would like to thank all my friends and family for always being there for me, with all their endless love and support, through the good and bad parts, I could not have done it without them.

Abstract

Tissue Engineering embraces the employment of novel biomaterials in order to realize functional tissue/organ repair or reconstruction. Graphene-based materials (GBMs) have attracted enormous interest due to their unique structure and properties, however, concern has been raised about their potential adverse effects. Therefore, it is of utmost importance to evaluate the cell-graphene interactions, as well as the underlying mechanisms in order to facilitate their proper development and use for biomedical applications.

In this thesis, we have studied two GBMs – graphene oxide (GO) and reduced graphene oxide (rGO) – and their effect on mesenchymal stem cells (MSCs), a pluripotent cell line extensively used in tissue engineering applications. We focused on whether the presence of these two materials activates the cellular oxidative stress response, a ubiquitous phenomenon related with disturbances in the normal redox state of cells. To determine the toxicity of graphene, cytotoxicity and proliferation assays were performed in cell cultures for different concentrations of GO and rGO. The localization of key transcription factors relating to the oxidative stress response was evaluated through immunofluorescent staining and confocal microscopy. The expression patterns of genes encoding for proteins of the glutaredoxin and thioredoxin cellular detoxification systems were also studied and analysed via quantitative RT-PCR, to detect potential alternations in mRNA expression caused by GO and rGO exposure. Through this work, we were able to determine that both GO and rGO affect cellular responses in a dose-dependent manner.

Keywords: biomaterials, graphene oxide, reduced graphene oxide, oxidative stress, MSCs, thioredoxin system, glutaredoxin system, cytotoxicity

Περίληψη

Η Μηχανική Ιστών ενσωματώνει τη χρήση καινοτόμων βιοϋλικών στοχεύοντας στην επιδιόρθωση της λειτουργίας ή την ανακατασκευή ιστών/οργάνων. Τα υλικά με βάση το γραφένιο (GBMs) έχουν προσελκύσει τεράστιο ενδιαφέρον λόγω της μοναδικής δομής και των ιδιαίτερων ιδιοτήτων τους, ωστόσο, έχει εκφραστεί ανησυχία για τις πιθανές δυσμενείς επιπτώσεις τους. Ως εκ τούτου, είναι υψίστης σημασίας να πραγματοποιηθεί αξιολόγηση των αλληλεπιδράσεων κυττάρου-γραφενίου, καθώς και των υποκείμενων μηχανισμών, προκειμένου να διευκολυνθεί η σωστή ανάπτυξη και χρήση τους για βιοϊατρικές εφαρμογές.

Σε αυτή τη διατριβή, μελετήσαμε δύο υλικά που έχουν ως βάση το γραφένιο – το οξείδιο γραφενίου (GO) και το ανηγμένο οξείδιο γραφενίου (rGO) - και την επίδρασή τους στα μεσεγχυματικά βλαστοκύτταρα (MSCs), μια πολυδύναμη κυτταρική σειρά που χρησιμοποιείται ευρέως σε εφαρμογές μηχανικής ιστών. Εστιάσαμε στο αν η παρουσία αυτών των δύο υλικών ενεργοποιεί την απόκριση του κυτταρικού οξειδωτικού στρες, ένα πανταχού παρόν φαινόμενο που σχετίζεται με διαταραχές στη φυσιολογική οξειδοαναγωγική κατάσταση των κυττάρων. Για τον προσδιορισμό της τοξικότητας του γραφενίου, πραγματοποιήθηκαν δοκιμασίες κυτταροτοξικότητας και πολλαπλασιασμού σε κυτταροκαλλιέργειες για διαφορετικές συγκεντρώσεις GO και rGO. Ο εντοπισμός των σημαντικών μεταγραφικών παραγόντων που σχετίζονται με την απόκριση του οξειδωτικού στρες αξιολογήθηκε μέσω ανοσοφθορισμού χρώσης και συνεστιακής μικροσκοπίας. Τα πρότυπα έκφρασης των γονιδίων που κωδικοποιούν πρωτεΐνες των συστημάτων κυτταρικής αντιοξειδωτικής δράσης - γλουταροξίνης και θειορεδοξίνης - μελετήθηκαν επίσης και αναλύθηκαν μέσω της ποσοτικής αλυσιδωτής αντίδρασης της πολυμεράσης με αντίστροφη μεταγραφάση (q RT-PCR), για να ανιχνευθούν πιθανές εναλλαγές στην έκφραση του mRNA που προκαλούνται από την έκθεση των κυττάρων σε GO και rGO. Στην παρούσα εργασία, μπορέσαμε να προσδιορίσουμε ότι τόσο το GO όσο και το rGO επηρεάζουν τις κυτταρικές αποκρίσεις συναρτήσει της συγκέντρωσης/δόσης του υλικού.

Λέξεις κλειδιά: βιοϋλικά, οξείδιο του γραφενίου, ανηγμένο οξείδιο του γραφενίου, οξειδωτικό στρες, μεσεγχυματικά βλαστοκύτταρα, σύστημα θειορεδοξίνης, σύστημα γλουταρεδοξίνης, κυτταροτοξικότητα

Table of Context

1. Introduction

1.1 Tissue engineering and regenerative medicine

During the last decades, Tissue Engineering (TE) and Regenerative Medicine (RM) have emerged as areas of great interest and research focus. They constitute interdisciplinary fields that integrate engineering, life sciences, cell and molecular biology to assemble functional constructs that restore, maintain, or improve damaged tissues or whole organs. While the fields are relatively new, the idea of creating artificial organs, tissues or even living organisms goes much further back in history. There are abundant references over the years in mythology, art and literature that feature people's desire to heal and restore injures and organs. Such an example is the well-known painting known as the "Healing of Justinian", which illustrates a miraculous transplantation of an artificial limb into an injured soldier by St. Cosmas and St. Damien. [1] The main principal of Tissue Engineering is to establish an appropriate combination of living cells and a three-dimensional (3D) microenvironment which act as templates for the development of substitute tissues and promotion of the endogenous regeneration human cells, tissues or organs (i.e., bone, blood vessels, cartilage, skin, muscle etc.) in order to re-establish normal functions and overcome organ transplantation downsides and limitations. The three components that TE consists of are: a) cells able to form a functional matrix, b) biocompatible porous scaffolds for transplantation and c) biologically active molecules, such as cytokines and growth factors. Regenerative Medicine is a broad field which includes TE and self-healing biological materials to regenerate cells or tissues. The fundamental concept of RM is to heal or rebuild tissues and organs damaged by age, disease, or trauma, as well as to correct congenital defects by reinforcing the organism's own regenerative capabilities.[2]

Nowadays, TE studies have turned their attention to stem cells – undifferentiated cells that have the ability of self-renewal, as well as a high differentiation potential into various cell types. There are two groups of stem cells according to their source: adult and embryonic stem cells. Stem cell populations are of utmost importance for TE applications, due to their capacity to self-renew without affecting their undifferentiated state and their ability to proliferate without limitations until they differentiate into a

specific cell type. A representative example of such cell population is Mesenchymal Stem Cells (MSCs). MSCs are multipotent stem cells with unique regenerative properties which can produce connective tissue cells *in vitro* and *in vivo* including bone, cartilage, and adipose tissue. They have gained increased attention as potential participants in transplantations and as regulator agents of immune-mediated rejection of transplants. [3] In this approach, the field of TE relies on the use of three-dimensional (3D), highly porous structures called scaffolds, to serve as a substrate for the implanted cells and as mechanical support to regeneration of tissues and organs. Scaffolds are designed to mimic the extracellular matrix (ECM) of the normal living tissue, incorporating biological signaling cues. The ideal scaffold should present the following characteristics: (1) high degree of porosity to facilitate cell migration, permit sufficient transport of oxygen/ nutrients and waste removal, (2) biodegradability in order to allow the production of native extracellular matrix from the cultured cells, (3) biocompatibility with a high affinity for cells to attach and proliferate and (4) strong mechanical properties consistent with the anatomical site. The biomaterials that are used for scaffold fabrication should be carefully selected depending on the tissue/organ of interest, as scaffolds interact with the cells at molecular level, influence cell functions and drive the complex cellular processes that lead to the development of a valid *in vitro* engineered tissue. However, this field comes with its intricate challenges and to achieve development and sustainability of tissues and organs, certain strategies need to be developed.[4]

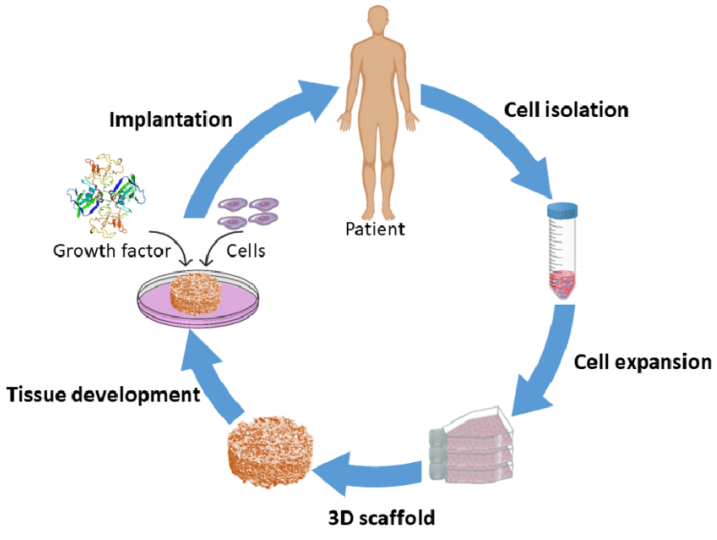

Figure 1. Schematic illustration of Tissue engineering procedure. [5]

1.2 Oxidative Stress

Oxidative stress is a phenomenon caused by a serious imbalance between the levels of ROS (Reactive Oxygen Species) in cells or tissues and their antioxidant defenses in favor of the former. The excess production of oxygen intermediates and/or the inadequate effectiveness of antioxidant defenses, disrupts the redox state of the cells, which is vital for their proper function, metabolism and signaling. Oxidative stress conditions, where the levels of oxidation are very high or very low, can subsequently lead to cell death by triggering regulated pathways that cause necrosis or apoptosis. Further, oxidative stress can cause severe damage and structural modifications in essential cell components, including lipids, proteins and nucleic acids, and it can also react with and affect surrounding biological tissues. The interference in the correct function of macromolecules often results in cellular dysfunction and degradation of cellular processes. In more detail, ROS can increase membrane fluidity and permeability by fragmenting the lipid membrane. Often the proteins are subjected to site-specific amino acid modification, peptide chain fragmentation, cross-linked reaction product aggregation, electric charge alteration, enzymatic inactivation, and proteolysis susceptibility by ROS action.[6] As for lipids, ROS can attack polyunsaturated fatty acids and cause lipid peroxidation, which in turn affects cell structures and can lead to more generalized adverse effects (for example, the oxidation of low-density lipoproteins (LDL) in the vascular endothelium is considered to be the mediator for the generation of atherosclerotic plaques and anomalies in cell metabolite transport). Last but not least, DNA oxidation, by reactions with free radicals, can evoke damage to DNA strands such as the denaturation of DNA strands, the alteration of nucleotides, the modification of bases and can even lead to the crosslinking of DNA-proteins. The mechanism of DNA oxidation can lead to mutagenesis and malignant cell transformation (cancer).[7]

From a medical perspective, oxidative stress in humans has been proposed to be associated with the process of aging, through mitochondrial DNA damage, as well as numerous of chronic diseases, such as neurodegenerative diseases (Parkinson's

disease, Alzheimer's disease, autism, multiple sclerosis etc.) cardiovascular diseases, diabetes and cancer.

Oxidative stress can result from:

- the presence of xenobiotics
- the activation of the immune system in response to invading microorganisms (inflammation)
- radiation, which makes oxidative stress a common denominator of toxicity or stress

Thus, to maintain intracellular homeostasis, a balance must be struck between the production of reactive oxygen species/accumulation of free radicals and the presence of antioxidant mechanisms that can detoxify the cell. The antioxidant system acts as a mediator to equilibrate the oxidative equivalents, prevent ROS formation and repair the damage they cause. The cellular antioxidant system includes both enzymes and non-enzymatic compounds that neutralize the high levels of free radicals.[7] Examples of such antioxidant molecules are glutathione, superoxide dismutase (SOD), catalase and other antioxidants such as ascorbic acid (vitamin C) and α-tocopherol (vitamin E)**,** whose actions aim to prevent ROS and their adverse effects on cells.

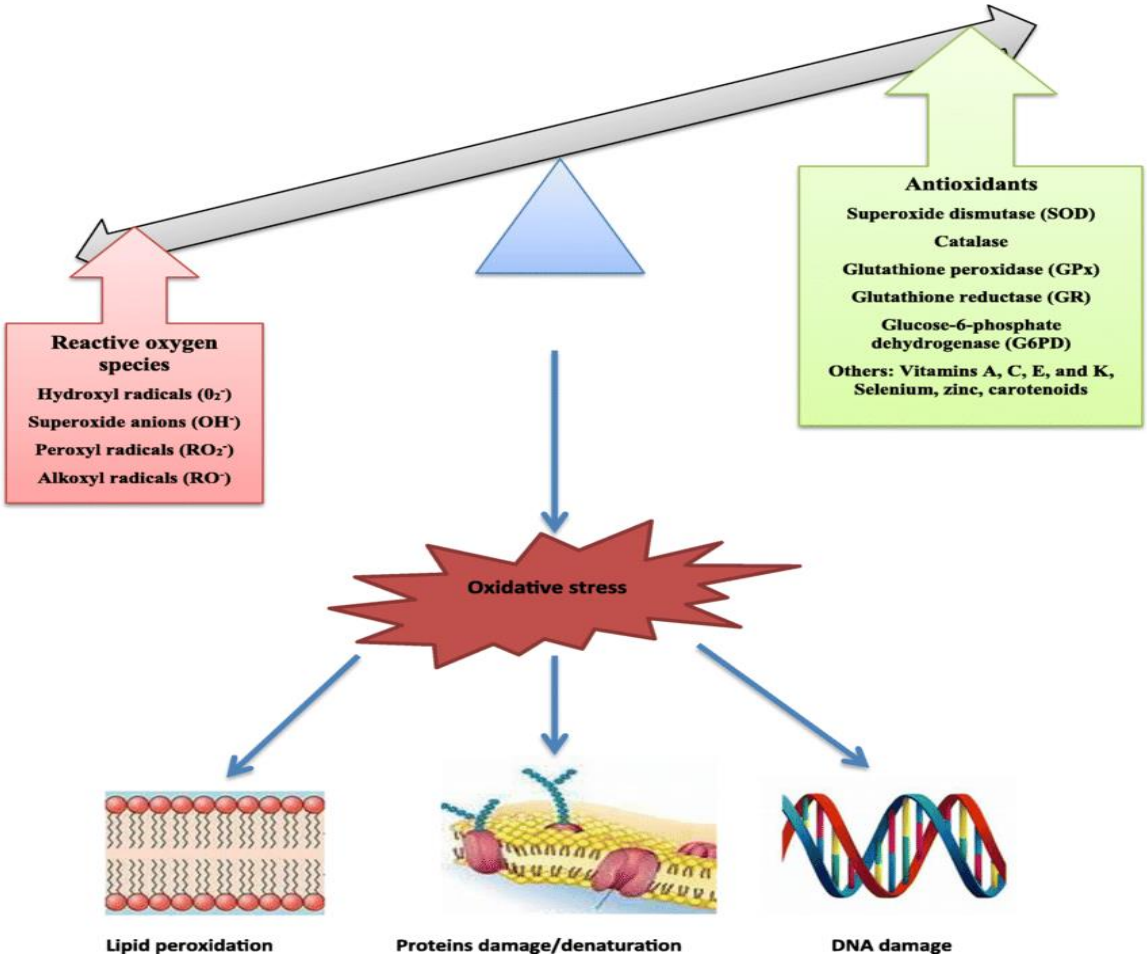

Figure 2: Oxidative stress base outline mechanisms [8]

1.2.1 Production of ROS

ROS generation can occur as a natural byproduct of normal aerobic metabolism through the mitochondrial respiratory chain, as, in low-levels, they are vital for cell metabolism. We refer to this type of reactive agents as intracellular free radicals. These molecules contain an unpaired electron and their molecular weight is low. The term ROS implies all those chemically reactive molecules derived from molecular oxygen (O_2), which has the ability to unpair to highly unstable and reactive free radicals.

Mitochondria are the main source of ROS production (approximately 90%) due to oxidative phosphorylation. Other major intracellular producers of ROS are the endoplasmic reticulum (ER) and peroxisomes through plasma membrane proteins (e.g., through NADPH oxidases), lipid metabolism and finally, a series of cytosolic enzymes.

In addition, ROS can occur as byproducts of the cellular response to ionizing radiation or physiological cellular processes for instance the creation of disulfide bonds.[7] ROS consisted of highly reactive (radical) molecules, such as the hydroxyl radical (•OH) and less reactive agents (non-radical) such as hydrogen peroxide (H_2O_2). When the oxidative equivalents react with biomolecules, free radicals are formed in a chain reaction. To eliminate this effect, interaction with other free radicals– so that uncoupled electrons are diminished – or antioxidant agents is needed.[9] The most common ROS forms are listed in the Table 1 along with the main sources of their generation.

ROS Molecule	Chemical Form	Main Source
Hydroxyl radical	(•OH)	Catalysis of hydrogen peroxide via metal ions Fe^{2+} or Cu^{2+} (Haber-Weiss reaction)
Superoxide	($O_2^{\bullet-}$)	One-electron reduction state, spontaneously forming in mitochondrial membrane and during other oxidation reactions Endogenously by xanthine oxidase (flavoenzymes) Activating mechanisms of phagocytic cells
Nitric oxide	(NO)	Enzymatic oxidation by nitric oxide synthase (NOS)
Hydrogen peroxide	(H_2O_2)	Two-electron reduction state of $O_2^{\bullet-}$ by NADPH-oxidase (neutrophils) Oxidation of transition metals by superoxide dismutase (SOD) Glucose oxidase
Perhydroxy radical	($HO_2^{\bullet}$)	Protonation of $O_2^{\bullet}$ by, more lipid-soluble

Table 1: List of most significant ROS and their prominent generation methods.

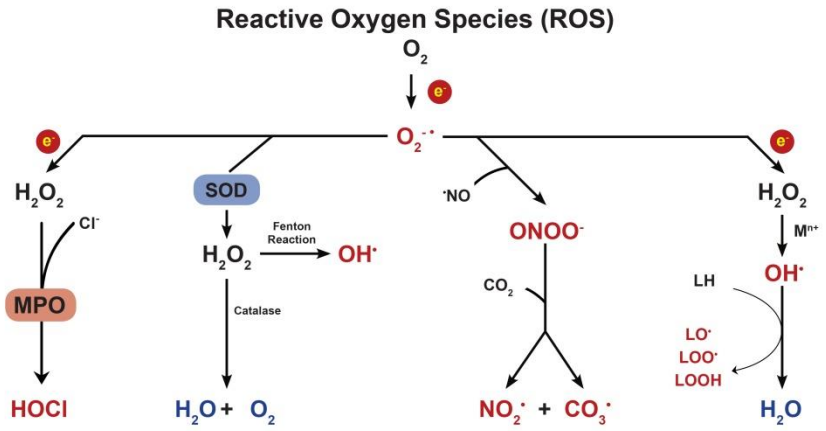

Figure 3: Schematic illustration of the oxygen reduction associated with ROS production. [10]

1.2.2 Defense Mechanisms against Oxidative Stress

Oxidative DNA damage repair is of utmost importance for the protection of normal cell function and in maintaining redox homeostasis. Due to this, the cell is equipped with a number of potential antioxidant mechanisms that are activated in response to elevated concentrations of ROS. The cellular antioxidative systems can be categorized into two groups: *enzymatic and nonenzymatic*.

Nonenzymatic antioxidants are mostly chemical molecules of low molecular weight that display antioxidative action. Primary representatives are Glutathione (GSH), ascorbic acid (Vitamin C), polyphenols and other substances. GSH or γ-glutamylcysteinylglycine, is considered the major ROS scavenger in oxidative conditions. After their synthesis, GSH molecules are distributed all over the cell.[9]

Enzymatic mechanisms involve various protein-based, enzymatic scavengers that promote degradation of ROS and develop specificity for particular ROS molecules, in order to mediate the intracellular oxidation. The redox balance is achieved by various reactions, which are shown in the corresponding sections.[11]

1.2.2.1 Superoxide dismutases

Superoxide dismutases (SODs) are a family of proteins that utilize different metal cofactors – and as such are known as metalloenzymes – in order to provide protection against the damage caused by superoxide anions. These proteins are responsible for the

metabolism of the superoxide anion free radical ($O_2^{\bullet-}$) into hydrogen peroxide (H_2O_2) and molecular oxygen (O_2). The reaction (Reaction 1) is followed by oxidation/reduction of the metal ions that are present in active location. The different forms of SODs are divided into four main groups: Copper-Zinc SOD, iron SOD, Manganese SOD and Nickel SOD and they are located in different cellular compartments. [12]

$$2O_2^{\cdot-} + 2H^+ = H_2O_2 + O_2$$

Reaction 1

1.2.2.2 Superoxide reductases

Superoxide reductase (SOR) is an iron-containing enzyme that has the ability to break down directly the reduction of superoxide radicals to hydrogen peroxide.

$$O_2^{\cdot-} + 2H^+ + e^- = H_2O_2$$

Reaction 2

1.2.2.3 Catalase

Catalases are heme-containing enzymes that catalyze the reaction of hydrogen peroxide into water and molecular oxygen. In mammalian cells, catalases are localized in peroxisomes where Reaction 3 takes place. Furthermore, they aim to minimize the chance of hydroxyl radical formation from H_2O_2 by other reactions catalyzed in the cell.

$$2H_2O_2 \rightarrow O_2 + 2H_2O$$

Reaction 3

1.2.2.4 Glutathione peroxidase

Glutathione peroxidase (GPx) is a cellular redox regulator expressed in low-level oxidative stress, which targets molecules that contain O_2^-, H_2O_2 groups (peroxide molecules), fatty acid hydroperoxides, and phospholipid hydroperoxides in mammalian cells. The 8 different isoforms of GPx are spread out in various subcellular compartments in different organs and tissues. These enzymes accomplish the reduction of H_2O_2 to water, and lipid peroxides to their alcohols.[13]

…In the present work we focused on the antioxidant defence systems of thioredoxin (TRx) and glutaredoxin (GRx). The two main thiol antioxidant systems are key factors of the redox homeostasis of the cell, as well as numerous physiological and biochemical functions, including the repair of DNA and proteins and sulfur metabolism. They are consisted of a group of redox proteins containing: thioredoxins (TRXs), glutaredoxins (GLRXs) and peroxiredoxins (PRDXs), which are ubiquitously expressed in various tissues and cells and they can be spotted in the extracellular fluid, the cytoplasm, the mitochondria and in the nucleus.

1.2.2.5 The Thioredoxin System (TRx)

The thioredoxin (Trx) system works alongside with glutaredoxin (Grx) system, both containing an active site with a redox-active disulfide and they are considered important constituent of the intracellular redox milieu. The Trx system consists of 3 main components: thioredoxins (Trx), thioredoxin reductases (TrxR) and nicotinamide adenine dinucleotide phosphate (NADPH), which play a key role in cellular redox homeostasis and signaling. Thioredoxins are able to carry out the reversible oxidation of protein-SH groups to a disulfide bridge (S-S) via thiol-disulfide exchange reaction. In essence, Trxs interact with thioredoxin reductases so they can obtain their reduced form and cause the reduction of target oxidized proteins. Consequently, the oxidized TrxR restores its reduced active-state via acquiring electrons from NADPH and react once again with the Trxs. Thus, Trxs as TrxRs allocate significant intracellular reactions such as ribonucleotide reduction fueled by the hydrogen donor NADPH though reduction mechanisms, accomplishing the proper prosecution of the applicable reaction. [14]

In mammalian cells, two thioredoxins (Txn1, Txn2) and three thioredoxin reductases (TrxR1, TxR2, TrxR3) are present. Thioredoxin 1 (Trx1) resides mostly in the

cytoplasm and nucleus and has a significant role in the reduction of oxidized proteins such as peroxiredoxins and ribonucleotide reductase. Thioredoxin 2 (Trx2) acts inside mitochondria, modulating the levels of mitochondrial ROS and helps prevent the activation of proinflammatory and apoptic pathways. Three TrxRs are found in mammalian cells: the cytosolic TrxR1, the mitochondrial TrxR2, and TrxR3, which was also termed thioredoxin/glutathione reductase (TGR) because it contains an additional N-terminal glutaredoxin (Grx) domain. TrxR3 action can be detected in the endoplasmic reticulum (ER), nucleus and cytosol. [15]

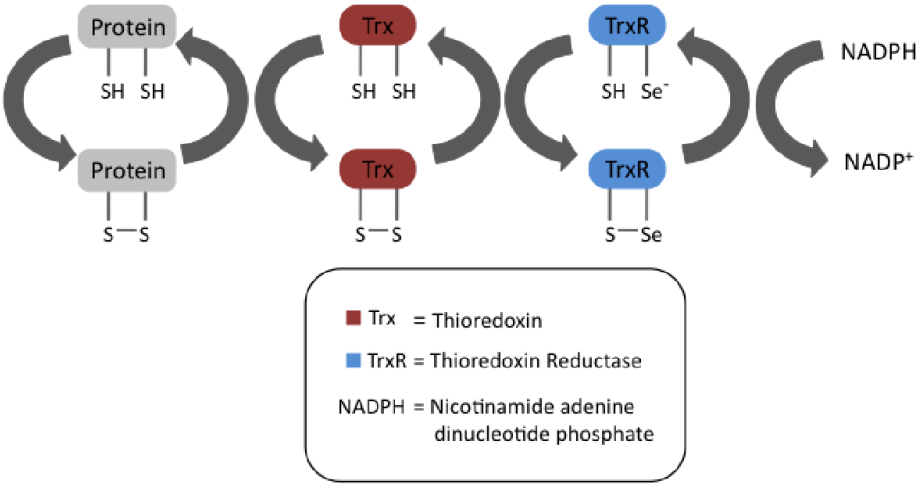

Figure 4: The Thioredoxin system as a redox regulator of protein function and signaling based on reducing cellular thiols. [16]

1.2.2.6 The Glutaredoxin System (GRx)

Glutaredoxins (GRxs) – just like TRxs – are ubiquitous small proteins that contain a redox-active disulfide. They have a large number of isoforms along the different species. These heat-stable enzymes catalyze thiol/disulfide or glutathione (GSH) mixed disulfides exchange through oxidoreduction reactions and therefore have a major role in the cellular defense against oxidative damage. In more detail, their oxidoreductase action contributes to regulating the levels of internal disulfide bridges in proteins and sulfur metabolism, particularly under conditions of oxidative stress. GRx proteins can function through either monothiol or dithiol mechanisms using one or two cysteines in their Cys–Pro–Tyr–Cys active site. Furthermore, they elicit the reversible oxidation of

two protein sulfhydryl groups (—SH) to a disulfide bridge (S=S) promoting electron transfer supplied from NADPH. [17]

The GRx system involves glutaredoxins (Grxs), glutathione (GSH), NADPH, glutathione reductase (Glr) and glutathione peroxidase (Gpx). The two main subsets of dithiol glutaredoxins present in mammalian cells are the cytosolic Grx1 and the mitochondrial Grx2 enzymes. Both oxidoreductases depend on glutathione (GSH) for their correct function but they participate in different catalytic mechanisms. Grx2 exhibits high affinity for glutathionylated substrates and electron donors, resulting in regulating mitochondrial redox defense especially against hydrogen peroxide (H_2O_2) stress, while Grx1 is considered a redox sensor that can control the level of the superoxide anion in cytosol.[18]

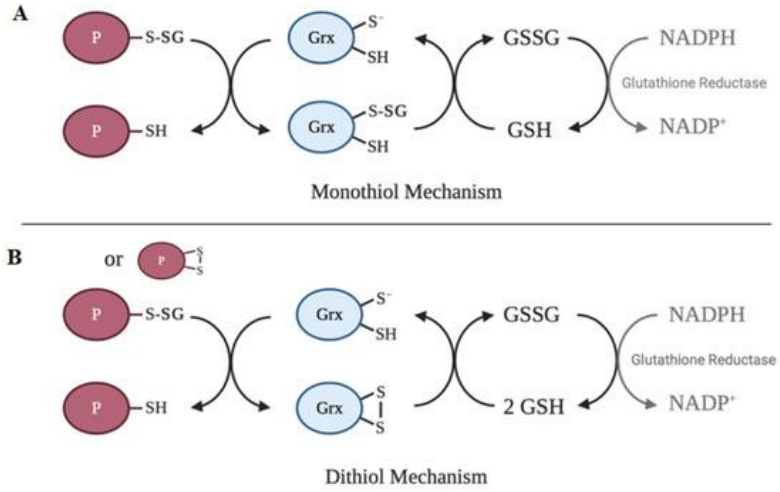

Figure 5: The two catalytic mechanisms of glutaredoxin system. (A) In monothiol mechanism, Grxs use only one active-site cysteine residue to reduce the mixed disulfide. Following the reduction of the enzyme intermediate by GSH to produce GSSG, that is reduced by glutathione reductase and NADPH. (B) In dithiol mechanism requires two active-site cysteines of glutaredoxin to reduce glutathionylated substrates. The oxidized Grsx acquire electrons from NADPH in order to, regenerate them to their active, reduced form in the presence of 2 GSH molecules.[19]

1.2.3 States of Oxidative Stress: Hypoxia and Hyperoxia

As mentioned previously, exaggerated or attenuated reactive oxygen species production can elicit the disturbance of homeostatic balance and subsequently results in oxidative stress conditions. Oxidative stress can be classified into two main states: Hypoxia and

Hyperoxia. Both are prominent features of pathological states that are detected by particular chemoreceptor cells and metabolic changes at the cellular level, that regulate the biochemical response which includes the induction of specific target genes. [20]

Hypoxia is defined by inadequate oxygen availability or supply at cellular, tissue and organ level, which arises when the oxygen demand surpasses oxygen supply. Low oxygen levels are sensed by the prolyl hydroxylase domain (PHD) proteins signalling pathway. This family of enzymes plays key role in the regulation of the transcription factor hypoxia inducive factor-1 (HIF-1) alpha. [21] HIF-1 is a heterodimer composed of HIF-1α and HIF-1β subunit proteins. HIF-1β is constitutively expressed in stable and low levels in specific cell types (myeloid cells, vascular endothelial cells, etc.), whereas the subunit HIF-1α is ubiquitously produced in all cell types. Under normal oxygen environment, specific proline and asparagine residues of HIF-1α are hydroxylated by PDH enzymes, ensuing ubiquitination and proteasomal degradation. When hypoxia occurs (O_2 concentrations of less than 6%), the hydroxylation of HIF-1α is prevented. As a result, HIF-α subunits translocate into the nucleus to bind with HIF-1β resulting in steady-state accumulation of HIF-1α protein. The activation of the HIF pathway elicits a series of adaptive responses, whose aim is to upregulate transcriptional cascades and reinstate tissue protection and adaptation. HIF-1α has a critical role in metabolically adapting the tissue to oxygen deprivation and anaerobic ATP synthesis, upregulation of glycolytic genes such as phosphoglycerate kinase (*PGK*) and is considered a direct target of redox regulation. [22]

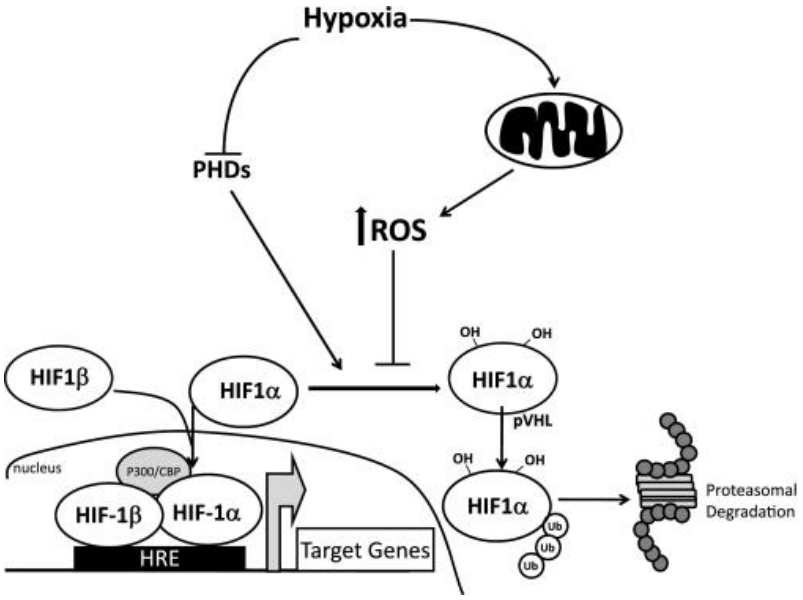

Figure 6: Schematic illustration of Hif-1α signalling pathway. Under basal conditions Hif-1α is constantly hydroxylated by PHD proteins causing its polyubiquitination and subsequently proteasomal degradation. When hypoxia occurs hydroxylation is inhibited, allowing the translocation of HIF-1α to the nucleus and couple with HIF-1 β, forming the active HIF-1 complex and promotes transcriptional activation of target genes. [23]

On the other hand, hyperoxia occurs when there is excessive oxygen supply. More specifically, the overproduction of ROS can evoke the attenuation of antioxidant defenses, resulting in oxidation of tissues and organs. The main sites, where ROS generation arises, are the nicotinamide adenine dinucleotide phosphate (NADPH) oxidase system and mitochondria. Hyperoxia induces the activation numerous intracellular signal transduction proteins, including transcription factors, channels, protein kinases and members of the apoptosic pathway. [24,25] A major regulator of this type of oxidative stress response is the nuclear factor erythroid 2 (NFE2)-related factor 2 (Nrf2), encoded by the NFE2L2 gene. Nrf2 belongs to the "cap 'n' collar" (CNC) subfamily of basic region leucine zipper (bZip) transcription factors, which also inhibits inflammation through the coordination of cytokine production and cross-talking with the nuclear factor-kappa B (NF-κB) redox signaling pathways. Nrf2 coordinates the expression of ROS-detoxifying enzymes through DNA sequences called antioxidant response elements (ARE), which include superoxide dismutase, catalase, glutathione S-transferase, NAD(P)H oxidoreductase, as well as the heme oxygenase protein (HO-1). At oxygen homeostasis (normoxia), Nrf2 is ubiquitously expressed and then degraded by the proteasome pathway, through interacting with its mediator, the repressor protein Kelch-like ECH-associated protein 1 (KEAP1). The latter ensures the localization of Nrf2 in the cytoplasm under normal conditions, while in oxidative conditions, the cysteine residues of KEAP1 are oxidized, the interaction with Nrf2 is inhibited, which then allows Nrf2 to translocate into the nucleus and transcriptionally activate a number of different genes. [26]

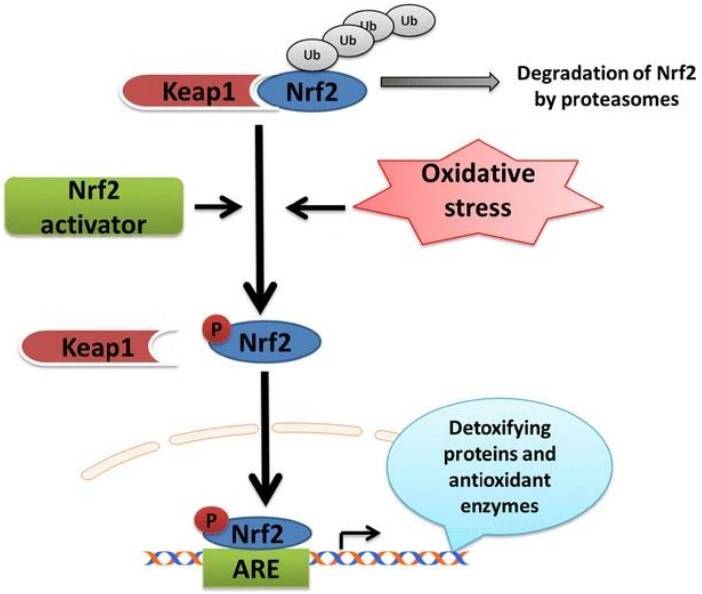

Figure 7: The Nrf2/Keap1 signal transduction in presence of oxidative stress. Under normal oxygen tension Nrf2 remains bound to Keap1 in the cytoplasm where it is targeted for ubiquitination and thereby degradation through proteasomal pathway. However, in oxidative conditions Nrf2 is separated from its repressor, phosphorylated and eventually translocate to the nucleus where it induces the anti-oxidative stress response. [27]

1.3 Graphene Family 2D Nanomaterials (GFNs)

Biomaterials are one of the three crucial components in tissue engineering, as they have the ability to provoke cellular functions, direct cell differentiation, and modulate cell-cell interactions. To achieve its goal, TERM (tissue engineering and regenerative medicine) aims towards the development of functional three-dimensional (3D) complex tissue constructs *in vitro,* which can mimic the cellular environment of tissue and may be used to repair or regenerate injured tissue/organ *in vivo*. [28,29] The generation of novel or improved graphene family nanomaterials (GFNs) has attracted a wide range of research interest in biomedical applications including bioelectronics, imaging, drug delivery, and tissue engineering. GFNs are a wide family of nanomaterials which are classified based on the number of layers in the sheet or their chemical modification and, as the term implies, they are comprised of graphene and its chemical derivatives. [28] In particular, the most prominent components of GFNs are graphene (G), graphene oxide (GO) as well as its reduced form, reduced graphene oxide (rGO), due to their extraordinary mechanical and electronic properties. Hence, graphene and its derivatives show excellent future perspectives for various clinical applications, such as in cardiac,

neural, bone, cartilage, skeletal muscle, skin/adipose tissue engineering and cancer therapy. [30]

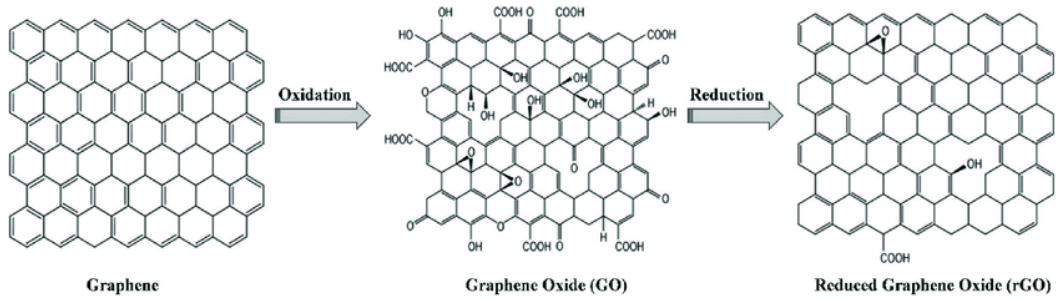

Figure 8: Basal backbone illustration of pristine graphene, graphene oxide (GO), and reduced GO structure along with the attached functional groups. [31]

1.3.1 Graphene as a biomaterial

Graphene is a single layer of graphite, composed of carbon atoms with sp^2 hybridized orbitals, bonded together in a planar 2D structure. Each carbon atom in the 2D nanomaterial creates covalent bonds with the three conterminous carbon atoms forming a hexagonal lattice crystal. This particular structure combined with its periodicity give exceptional electrical and strong mechanical characteristics to the material. Additionally, graphene features superior physical and optical properties including hardness, high surface area, excellent electrical and thermal conductivity, chemical stability, elastic modulus at the ratio of 1 TPa and pliability. [32] Among others, graphene stands out as one most promising candidate in TE due to its biocompatibility and ability to interact with bioactive compounds such as proteins, enzymes, drugs, growth factors, and DNA. Furthermore, owing to the ultra-high surface area and its electron mobility, graphene and its derivatives are utilized in the development of artificial scaffolds that can be applied in a wide number of tissue engineering applications, such as: vascular, bone, neural, and tendon/ligament TE. However, many studies have indicated that graphene can induce toxicity pathways by reactive oxygen species generation, which can be dependent on a number of different parameters, including concentration, time of exposure, size and shape, resulting in cellular oxidative stress. [33] Therefore, the toxicological potential of graphene and its components required further investigation.

1.3.2 Graphene Oxide and its chemical properties

Graphene oxide (GO) is a highly oxidized form of graphene and its conformation comprises a single atom layer and abundant surface functional groups such as carboxylic acid, epoxide, and hydroxyl groups. It is characterized by high catalytic activity and its large surface area and π-conjugated structure facilitates cellular interactions. The introduction of functional groups on its surface offers GO hydrophilicity, dispersibility and therefore enhances its bioavailability.[34] Those functional groups enable the conjugation of GO to other molecules and polymers, thus enhancing its mechanical, physical, and electrical properties. This, combined with its vast surface area, promote the adsorption of various proteins and adhesion to cells. In addition, the amphiphilic character of GO can be used as a surfactant to stabilize hydrophobic molecules in a solution. [35] Compared to graphene, GO is considered a more efficient material due to its advantageous dispersibility in aqueous media, smaller size, high biocompatibility, accessibility, hydrophilicity, chemical tunability and processability. [36] In this regard, many studies have indicated GO as an ideal biocompatible approach that can be widely utilized in TE, for applications focusing on cell-adhesion substrates, the delivery of growth factors for cell cultures and differentiation protein-delivery carriers to facilitate the differentiation of various stem cells. Recently, *Safina and co-workers* reported that pristine graphene and two forms of oxidized graphene films (high- and low oxygen) could participate in skin regeneration strategies, as they presented low cytotoxicity and skin cell proliferation and differentiation. [37] Additionally, GO and its reduced form (rGO) exhibit excellent osteogenesis-inducing capability, as well as mechanical support and have been employed in bone tissue engineering scaffolds together with other biomaterials, such as hydroxyapatite, gelatin hydrogel, calcium phosphate and others. [38]

1.3.3 Reduced Graphene Oxide and its chemical properties

The reduced form of graphene oxide (rGO) is a versatile biomaterial which can be obtained by thermal, chemical, or UV exposure processes, in order to diminish the oxygen-containing functional groups on the surface. [39] Each procedure of reduction offers different properties to the produced rGO, so the appropriate method needs to be

selected according the final application for which it is intended. For the employment of rGO in tissue engineering applications, it is important to take advantage of non-toxic and environmentally friendly reducing agents (e.g. ascorbic acid) for its production.[40] Similarly to GO, rGO can promote protein adsorption and cell-cell or cell-matrix interactions due to its electrical properties and increased electron mobility. The reduction of GO endows the biomaterial with electrical conductivity and hydrophobicity, which enhances cell−material interactions related to the regulation of major biological processes including inflammatory responses. Due to its inherent biocompatibility biodegradability, antimicrobial activity and pro-angiogenic properties, this biomaterial could also be used in the development of safe (and environmentally-friendly) platforms for cell culture studies.[41] Even after the reduction, rGO still retain a few oxygen-containing groups, as a result of incomplete reduction and defect formation. Its low oxygen content in the surface facilitates material's further modulation, regain some of graphene's properties and endow rGO with high electronic conductivity and thermal stability. Compared to GO, its structural modifications allow rGO to establish interactions with biomolecules, cells and polymers. Therefore, rGO has been widely integrated in composite scaffolds for neural or cardiovascular applications, providing the appropriate extracellular microenvironment and enhancing cellular behaviors (e.g., adhesion, proliferation, and migration). Other studies established that the incorporation of those biomaterials in three-dimensional (3D) structures which can mimic the neural microenvironment, while exhibiting excellent biological, electrical and mechanical properties. *Girão et al.* investigated the performance of 3D rGO-incorporated scaffolds organized in porous networks whose surfaces were enhanced with biocompatible nanofibers. Results demonstrated that those fibrous-porous structures are able to promote the regenerative potential of neural circuits *in vitro* and thus, restore their functional activities.[42] However, studies have reported that rGO can induce dose-dependent toxicity resulting in oxidative stress to various cell lines. A number of groups have studied the correlation between cytotoxicity and the physiochemical properties of GO and rGO. In this respect, *Das et al.* demonstrated that GO exhibits higher levels of toxicity and increased DNA damage than reduced GO at the same size, while others indicate that rGO could cause more membrane disruption and oxidative stress than GO. [43] The results indicated that both nanomaterials (GO and rGO) provoked an increased intercellular generation of ROS

and messenger RNA (mRNA) expression of heme oxygenase 1 (HO1) and thioredoxin reductase (TrxR), pointing towards oxidative stress induction. Nevertheless, the authors suggested that potential interference in the functional group density of GO could eliminate cellular cytotoxicity via careful modulation of the GO reduction while preserving its solubility.[44] In this perspective, it is crucial to determine the way lateral dimensions, functional groups and redox activity of the produced rGO affect the *in vitro* cytotoxic behaviors and underlying molecular mechanisms.

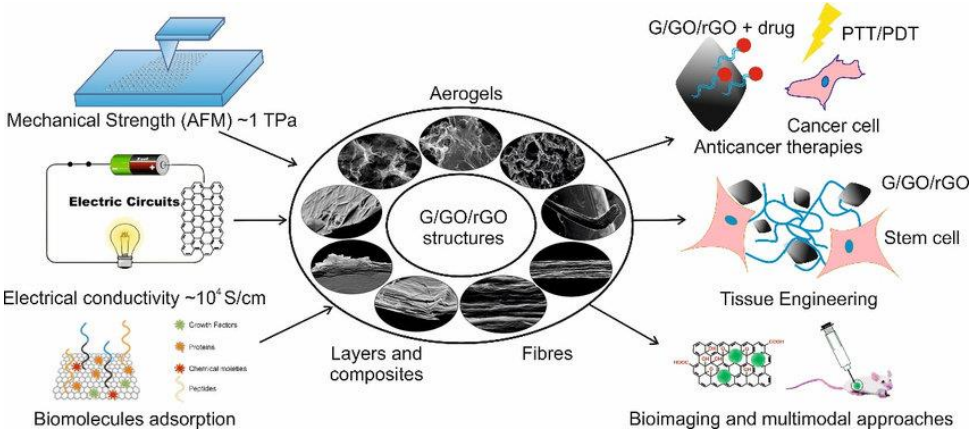

Figure 9: A brief schematic diagram of multiple biomedical applications and mechanical, electrical, and biological exceptional properties of graphene (G), graphene oxide (GO), and reduced graphene oxide (rGO) including authors SEM images from graphene oxide forms (paper, aerogels and fibres). [45]

1.4 Mesenchymal Stem Cells (MSCs)

Stem cells (SCs) can be defined as undifferentiated cells which are able to proliferate and establish daughter cell lines for tissue generation. They are at the forefront of regenerative cell studies due to their distinctive features: excellent self-renewal capability and the ability to differentiate into one or more specialized cell lineages, also known as potency. Stem cells can be distinguished in the following populations according to their respective developmental potential: a) unipotent (can differentiate into a single cell type), b) multipotent (have the ability differentiate into a few cell types), c) pluripotent (are able to differentiate into all three germ layers; endoderm, mesoderm or ectoderm) and d) totipotent (can form all cell types). [46],[47] According to their source of origin, stem cells can be classified into three main categories: 1)

Embryonic stem cells (ESCs) are derived from the mammalian embryonic tissue, with the ability to be developed into almost all cell types; ESCs are characterized by pluripotent differentiation potential and extensive proliferation 2) Adult/stromal or postnatal stem cells (ASCs), are multipotent progenitor cells which are extensively distribute in numerous adult tissues including bone marrow, bone, skin, blood vessels, and muscle, mesenchymal stem cells (MSCs), They have the capacity to differentiate into other cellular lineages beyond their tissue(s) of origin. 3) Induced pluripotent stem cells (iPS) can be obtained by genetic manipulation of somatic differentiated cells into a dedifferentiated state resembling embryonic stem cells. [48] Moreover, they contribute in the preservation of intracellular homeostasis within the tissue and include a high-quality repair with regeneration of the injured tissue or organ.[49] A great number of studies have reported that SCs differentiation pathways can be induced with the involvement of certain soluble factors such as growth factors, hormones and other small biomolecules, and certain physical cues. According to their localization and functions, cells are subjected to numerous physical cues (*in vivo)* or experimental conditions (*in vitro)*, so they become tissue or organ-specific cells owning distinctive functions and consequently provide precursor agents for treatment of degenerative, malignant and genetic diseases.[50]

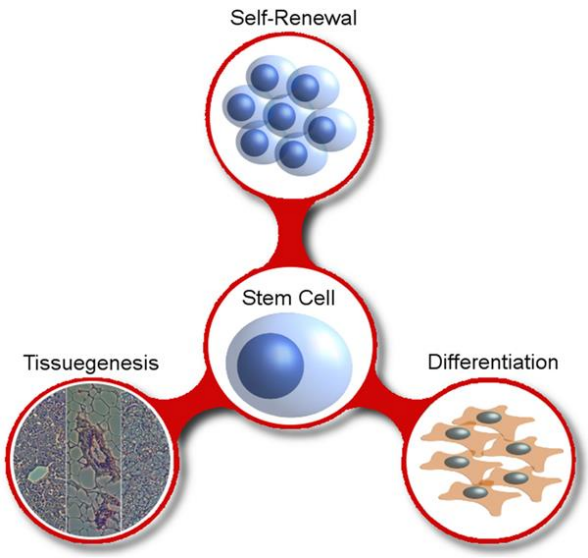

Figure 10: Fundamental properties of stem cells (SCs). Stem cells are defined by three major properties. 1) self-renewal: the cellular action that involves proliferation to produce daughter cells while preserving both multipotency and tissue regenerative potential. 2) Differentiation: the ability to differentiate into

various phenotypes of functional cells. 3) Tissuegenesis: the production of the multiple cell types of their given tissue resulting in tissue regeneration. [51]

A particular subtype of multipotent stem cells, adult mesenchymal stem cells (MSCs), have gained tremendous attention over the past few years in the field of tissue engineering and regenerative medicine, due to their exceptional therapeutic potential for use in clinical therapies and research. They were initially identified as clonogenic fibroblast precursor cells (CFU-F), isolated from whole bone marrow owning the ability to form bone- and cartilage-like colonies, by Friedenstein and colleagues in 1970. [52] Eventually, in the early 90's, the term 'mesenchymal stem cells' was introduced by Caplan to the subpopulation in bone marrow that possess the ability of self-renewal and differentiate distinctive end-stage cell types, such as those that fabricate specific mesenchymal tissues such as bone, cartilage, muscle, bone marrow stroma, tendon/ligament, fat, dermis, and other connective tissues. [53] MSCs can be isolated from a broad range of tissues, including umbilical cord, endometrial polyps, menses, bone-marrow, blood, adipose tissue etc. Hence, the ease of harvest and quantity acquired enable the exploitation of these cells vastly in cell-based tissue engineering strategies, especially in tissue regeneration and repair under localized or systemic conditions. [54] They exhibit related anti-inflammatory, trophic, paracrine and immuno-modulatory functions. Another advantage of this cell type is their capacity of secreting and regulating a wide spectrum of bioactive agents at heterogeneous concentrations depending on the signals secreted due to injury, infection or local microenvironmental cues. MSCs can either be transplanted autologous (auto-transplantation) or be seeded in biocompatible scaffolds, and then implanted into the organism to repair the potential defect. Due to their unique immunosuppressive, regenerative properties, rapid proliferation and multipotency, MSCs are considered exceptional cell candidates for tissue engineering and regenerative medicine therapies, including skin therapies, organ transplants as well as maintenance of cancerous cells. [55]

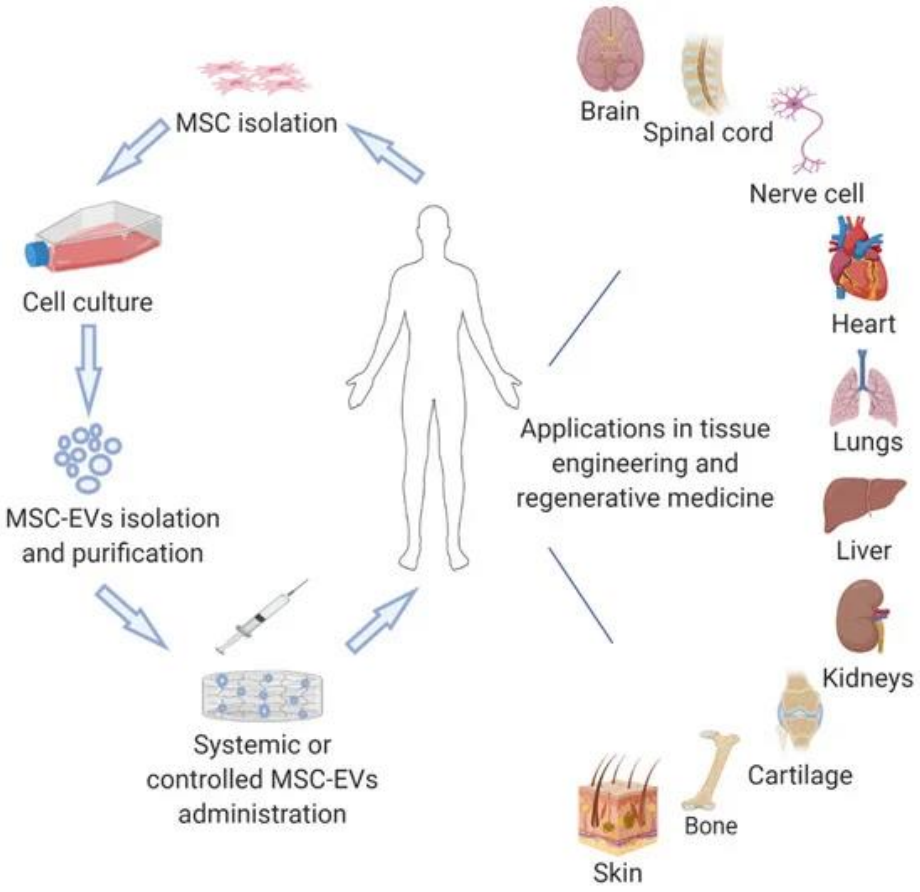

Figure 11: Schematic diagram of the multipotentiality and potential applications of mesenchymal stem cells (MSCs) in tissue engineering and regenerative medicine. [56]

2. Materials & Methods

2.1 Cell Cultures

All experiments in this study were conducted with murine bone marrow-derived Mesenchymal Stem Cells (MSCs). The cells were grown and maintained in low glucose (1000mg/L) Dulbecco's modified Eagle's culture medium (DMEM) supplemented with 10% fetal bovine serum (FBS) and 1% penicillin/streptomycin solution (PS) and incubated at 37 °C in a humidified atmosphere with 5% CO_2. Experiments were carried out with cells of low passage number (between P2 and P8) in order to avoid interassay variability, with medium changes every 2-3 days.

2.2 GO & rGO Solutions

In the present study, both graphene oxide (GO) and reduced graphene oxide (rGO) solutions were used in order to evaluate the cellular mechanisms that are activated upon exposure. Both GO and rGO dispersions that were used in this work were fabricated by associates from the Hellenic Mediterranean University (HMU), who firstly fabricated graphite oxide using a modified Hummers method, subsequently produced GO monolayers through ultrasonication and finally, reduced the GO with ascorbic acid (vitamin C) to create rGO.

Fabrication of graphene oxide (GO)

Briefly, graphite oxide was obtained by mixing 1g graphite powder with 46 mL H_2SO_4 in a beaker and kept for 20 min. under vigorous stirring. Then, the mixture was transferred to an ice bath for 20 min, followed by slow addition of $NaNO_3$ for 1 h under continuous stirring. 6g $KMnO_4$ were added in small portions and the color of the mixture turned into deep green. The insoluble matter was kept under continuous agitation overnight. After 24 h the mixture turned a dark brown color. The next day the mixture was heated at 35^{o}C under stirring for 1 h and 40 min. Then the temperature was increased to 90^{o}C with the gradual addition of 80 mL dH_2O and kept under consant stirring for 40 min. The beaker was then removed from the heat and the mixture was diluted with 200 mL of distilled water. Then, 20 mL of H_2O_2 solution (30%) were added dropwise into the beaker, changing the color of the mixture to green-brown and generating froth due to oxygen production. The suspension was left stirring until it reached room temperature (25^{o}C). The mixture was then centrifuged at 4200 rpm for 20 min. The supernatant was removed and the solid matter was washed with hot distilled water (at 65^{o}C). The undissolved substance was then washed with deionized water until it was neutral (pH=7) and was left to dry under vacuum at 50^{o}C resulting in graphite oxide. The exfoliation of graphite oxide to GO sheets was performed by sonicating the graphite oxide dispersion, using an ultrasonication probe, for 1 h on ice. The GO dispersion was obtained after centrifugation at 4200 rpm for 30 min in order to remove the unexfoliated GO sheets, with the final concentration of the GO dispersion adjusted to 1mg/mL with dH_2O.

Chemical reduction of graphene oxide (rGO)

The reduced form of GO can be obtained by a wide variety of reduction processes/ techniques such as thermal reduction, solvothermal reduction, electrochemical reduction, chemical reaction reduction etc. In this case, the reduction of GO was achieved through the use of ascorbic acid, also known as Vitamin C (VitC). More specifically, 20 mL of GO solution were mixed with 200 mg ascorbic acid (molar ratio of 1:10). The resulting suspension was kept under vigorous stirring at RT for 48 h. Next, the suspension was centrifuged at 4200 rpm for 30 min and washed 2 times with deionized water. The precipitate was left to dry under vacuum at 50^{o}C.

Characterization of reduced Graphene Oxide

The synthesized rGO dispersion was characterized with a number of instrumental methods. Attenuated Total Reflectance Infrared Spectrometry (ATR-IR) measurements were carried out to determine the chemical reduction degree of rGO using Bruker Vertex 70v FT-IR. The samples were tested in solid state. The reduction of the samples was determined UV-Vis spectroscopy by Shimadzu UV-2401PC ultraviolet-visible spectrometer in diluted dispersions of GO & rGO samples. Further structure characterization was performed using Raman spectroscopy at room temperature via Horiba LabRAM HR Evolution spectrometer, where samples were examined in solid state. Thermal stability of rGO was investigated with thermogravimetric analysis (TGA) using 4mg samples in temperature ratio of 50-800 °C, at a heating rate of 10˚C/min by Perkin-Elmer Diamond Pyris spectrometer. Finally, element information was obtained using Wavelength-dispersive X-ray spectroscopy (WDXS).

L-ascorbic acid (Vitamin C) as a reducing agent

Chemical reduction of the dispersed GO sheets can be accomplished by several reductants, including, hydrazine, dimethylhydrazine, hydroquinone, sodium borohydride and hydrohalic acids. The majority of those reductants are considered highly toxic, corrosive, potentially explosive and are likely to cause environmental and health issues.[57] Consequently, new approaches that involve more ‘green’, inexpensive and nontoxic reagents have been developed. L-Ascorbic acid (L-AA), is a natural antioxidant essential for many metabolic functions in living organisms and extensively employed as a food additive. [58] Recent studies have revealed that vitamin C is an eco-friendly and harmless reagent - as it does not generate contaminants during the

reduction process - that can replace hydrazine for effective reduction of graphene oxide. Besides its pronounced reduction capability to graphene oxide, Vitamin C presents capping action which allows the simultaneously stabilization of the reduced GO sheet while being able to reduce the GO without using additional capping reagents. [59]

Figure 12: Digital picture of GO & rGO dispersions.

2.3 MTT Viability/Proliferation Assay

The evaluation of cell viability and proliferation of both GO and rGO solution was achieved by using the *in vitro* colorimetric MTT Assay. In more detail, MTT or 3-(4,5-dimethylthiazol-2-yl)-2,5-diphenyltetrazolium bromide is a yellow tetrazolium salt that is reduced to purple formazan crystals by metabolically active cells. The viable cells contain oxidoreductase enzymes that are responsible for the reduction of MTT to formazan. The greater the number of viable cells, the higher the number of formazan crystals formed and, therefore, the greater the degree of light absorbance.

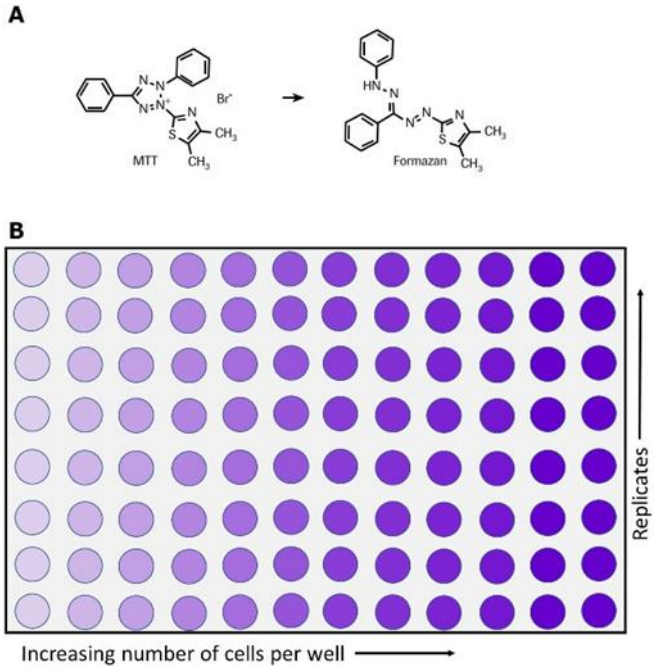

Figure 13: A) MTT's reduction to formazan crystals. B) Schematic illustration of 96-well plate during MTT Assay. [60]

Briefly, MSCs were seeded in 96-well flat-bottom culture plates at a density of 3x10^3 cell/well 100µL culture medium. After 24 h of culture at 37 ^{O}C and 5 % CO_2 in a humidified incubator, the supernatant was removed. Then, treatments to be tested (specifically 1 µg/mL, 5 µg/mL, 10 µg/mL, 25 µg/mL, 50 µg/mL, 100 µg/mL of both GO and rGO) were performed in triplicate. The above concentrations were tested using media with FBS (+) and without FBS (-). As a positive control, 3 wells were treated with low-glucose medium +/- FBS. After a further 24 and 48 hours of incubation, the treatments were removed and the cells were washed 3 times with 1xPBS +/+ (phosphate buffered saline) (containing Mg^{2+} and Ca^{2+} ions). A working MTT solution was prepared to a final concentration of 0.5 mg/mL, using DMEM without FBS (due of the potential interference of FBS during the absorbance measurement). The MTT solution was added directly to the samples and was left for 4 hours at 37^{O}C and 5% CO_2. Following the removal of the supernatant, 100µL per well of DMSO-isopropanol (at a 1:1 ratio) solution were added to the samples and left to incubate for 15 minutes at room temperature (RT) and then for another 15 minutes at 4^{o}C. Finally, the absorbance was measured at wavelength of 545 and 630 nanometers using a microplate ELISA reader.

2.4 Live/Dead Assay

For the assessment of cytotoxicity of GO & rGO solutions, the two-color LIVE/DEAD™ Viability/Cytotoxicity Assay Kit for mammalian cells was used. In this case, MSCs were cultured in 24-well plates containing glass coverslips to a density of 5x10^4 cells/mL. The cells were incubated at 37^{O}C and 5 % CO_2 for 24 and 48 hours as described above, followed by medium removal and washing once with 1xPBS. GO and rGO treatment was performed in duplicates, with medium plus and minus FBS, at the concentrations of: 0 μg/mL, 10 μg/mL and 100 μg/mL. The samples were left to grow at 37^{O}C and 5 % CO_2 in a humidified incubator overnight. The positive control samples were treated with DMEM only and the negative control sample with H_2O (where all cells are expected to die due to osmotic shock). The next day, the treatment was removed and the cells were washed once more with 1xPBS. Live/Dead solution was prepared by adding 12 μL of the 2 mM ethidium homodimer-1 (EthD-1) stock solution and 3 μL of the 4 mM calcein AM stock solution to 10 mL of non- sterile 1xPBS, (in order to reach final concentrations of 4 μM EthD-1 and 2 μM calcein AM). Subsequently, the solution was added to the samples at a final volume of 300 μL/well and left for 45 min at RT. After the Live/Dead solution was removed, samples were fixed with 4% paraformaldehyde (PFA) for 15 min at RT and then, washed three times with 1xPBS. As a final step, the coverslips were counterstained and carefully mounted on microscope slides using mounting medium containing DAPI.The samples were observed using an epifluorescent microscope and fluorescence images for live (green staining due to calcein AM) and dead (red staining due to EthD-1) cells were obtained.

2.5 Immunocytochemical Assay

For this assay, MSCs were seeded under the same standardized culture conditions and density as described above in the Live/Dead assay. The culture medium was removed from the wells and treatment was performed in duplicate for the concentrations of 5 μg/mL and 50 μg/mL GO & rGO, along with 200μM Hydrogen Peroxide (H_2O_2) as a positive control and DMEM alone used as negative control. The timepoints that were examined are divided into two groups: A and B. In group A, the treated cell cultures were incubated for 1h and 4h while, in group B, they were incubated for 24h and 48h.

After the desired incubation time was reached for each case, cells were washed once with 1xPBS (+/+), and then fixed with 4% PFA for 15 min. Samples were then washed three times with 1xPBS, which was followed by permeabilization of cell membranes using 0.1% Triton X-100 in 1xPBS for 5 min. Non-specific binding sites were blocked with 2% BSA in 1xPBS for 1 hour. Primary antibodies were added at optimum concentrations in 0.5% BSA and 0.1% Triton X-100 in 1xPBS and samples were incubated overnight at 4^{o}C (Table 1). At the end of the incubation period, cells were washed 3x with 1xPBS and labeled with the corresponding secondary antibody in 0.5% BSA and 0.1% Triton X-100 in 1xPBS for 1h at room temperature (RT). Phalloidin 555 or 680 (1:750) was also added in the same step. After the samples were washed 3x with 1xPBS, they were mounted onto microscope slides with an antifade mounting medium containing DAPI for nuclei counterstaining. DAPI (4′,6-diamidino-2-phenylindole) is a highly specific DNA stain which emits blue fluorescence upon binding strongly to A-T rich regions in DNA to form the fluorescent complex. This fluorescent dye can pass through an intact cell membrane thus, both live and fixed cells can be stained, though less effective in live cells as it is unable to efficiently pass through the membrane. Therefore, provides a marker for membrane viability. Cell imaging was performed using a Leica SP8 Confocal Microscope. The primary and secondary antibodies used in this thesis can be seen in Table 1 along with their conditions of use.

Table 1: List of the antibodies used in the current study.

Primary Antibody	Conditions of use	Secondary Antibody	Conditions of use
Hif1-a	1:800	a-rabbit 687	1:500
Ki67	1:800	a-mouse 488	1:500
Nrf2	1:800	a-rabbit 555	1:500

2.6 Real Time Reverse Transcription Polymerase Reaction (RT-qPCR)

This method was used to elucidate whether the presence of GO and rGO in the growth medium could affect the oxidative state of cells by evaluating the up- or downregulation of certain genes involved in the oxidative stress response. Total RNA was isolated from MSCs after 24h and 48h of exposure to different concentrations of GO and rGO, using DMEM both with and without added FBS. The validation of all RNA samples was determined with NanoDrop® ND-1000 Spectrophotometer.

2.6.1 RNA isolation

For the isolation of total RNA from MSC cultures, the following process was followed:

Lyse sample and separate phases

1. Samples were lysed and homogenized in TRIzol™ Reagent according to the following protocol.
    a. Cells were centrifuged and the supernatant was removed.
    b. The dose of 0.75 mL TRIzol™ Reagent was added to the pellet per 0.25 mL of sample (5 x 10^6 cells).
    c. The lysate was pipetted up and down several times in order to homogenize.
2. Cells were incubated for 5 min to permit complete dissociation of the nucleoproteins complex.
3. The dose of 0.2 mL of chloroform was added per 1 mL of TRIzol™ Reagent used for lysis and then the cube was capped securely.
4. Samples were incubated for 2-3 minutes.
5. Following the centrifugation of the samples for 15 minutes at 12,000 x g at 4 °C. At the end of the centrifugation, the mixture was separated into a lower red phenol-chloroform, interphase and a colorless upper aqueous phase.
6. The aqueous phase containing the RNA was transferred to a new tube.
7. The aqueous phase containing the RNA was transferred again by angling the tube at 45° and then pipetted out to a new tube.

RNA Isolation

1. The precipitation of the RNA was conducted as follows:
    a. 0.5 mL of isopropanol were added to the aqueous phase, per 1 mL of TRIzol™ Reagent used for lysis.
    b. Samples were incubated for 15 minutes
    c. The centrifugation of the sample was followed for 10 minutes at 12,000 x g at 4 °C. Total RNA precipitate formed a white gel-like pellet at the bottom of the tube.
    d. The supernatant was discarded with a micropipettor.
2. The wash of RNA was executed.

a. Pellet was resuspended in 1 mL of 75% ethanol per 1 mL of TRIzol™ Reagent used for lysis.
b. Samples were vortexed briefly and then centrifuged for 5 minutes at 7500 x g at 4 °C.
c. The supernatant was removed with a micropipettor.
d. The RNA pellet was allowed to air dry for 5-10 minutes.

3. The solubilisation of RNA was carried out.
    a. The pellet was resuspended in 20-50 µL of RNAase-free dH_2O with 0.1 mM EDTA by pipetting up and down.
    b. RNA was incubated in heat block set at 55-60° for 10-15 minutes.
4. Finally, the RNA yield was determined by absorbance measurement using a NanoDrop™ at 260 nm and 280 nm.

2.6.2 Complementary DNA (cDNA) synthesis

For the synthesis of cDNA from 4000 ng of total RNA in this study, two different mixtures to final volume of 10 mL each were prepared according to protocol. The recipes that were followed for the preparation of the mixtures are displayed on table 2.

Table 2: Recipes for the preparation of cDNA mixtures

RNA Mix	
OligoTT	1 µL
dNTPs	1 µL
RNA	X µl
dH2O	8-x µl

cDNA synthethis mix	**For 1 RNA sample**
5x RT buffer	4 µL
50 mM $MgCl_2$	2 µL
0.1 M dTT	2 µL
RNase Out	1 µL
Super Script III RT	1 µL

cDNA synthesis comprises of three distinct stages:

1. RNA denaturation: Once the RNA mixes were prepared for each RNA sample in PCR microtubes, they were incubated at 65^{O}C for 5min using a Veriti™ 96-well Thermal Cycler (Applied Biosystems Life Technologies, Foster City, CA,

USA).

2. Primer extension and cDNA synthesis: The tubes were removed from the Thermal Cycler and left on ice for 1 min. Then, 10 μL of cDNA synthesis mix were added to each tube and the samples were returned to the thermocycler to continue the reaction at 50^{O}C for 50 min.

3. Reaction termination: The samples were incubated at 85^{O}C for 5 min. When finished, the cDNAs were stored at -20 ^{O}C until the next step of the experiment.

All experiments in this thesis were carried out with cDNA obtained using only the method described above.

2.6.3 Primers – Genes

For the assessment of oxidative stress in mRNA expression, genetic expression analysis was performed on a selected number of target genes. Glyceraldehyde-3-phosphate dehydrogenase (Gapdh) was used as a reference gene. The symbol, full name, and type of target genes that were studied in the present thesis are listed in Table 3. Appropriate primer pairs (forward and reverse) for qPCR were chosen according to protocol, the sequence and melting temperature (T_m) of the primers used can be seen in Table 4.

Table 3: Summary of the target genes used in this study

Symbol	Name	Localisation
GAPDH	Glyceraldehyde-3-phosphate dehydrogenase	Cytosol
Glrx1	Glutaredoxin 1	Cytosol
Glrx2	Glutaredoxin 2	Nucleus / Mitochondria
Txn1	Thioredoxin 1	Cytosol / Nucleus
Txn2	Thioredoxin 2	Mitochondria
Txnrd1	Thioredoxin Reductase 1	Cytosol
Txnrd2	Thioredoxin Reductase 2	Mitochondrial
Txnrd3	Thioredoxin Reductase 3	Endoplasmic Reticulum (ER) / Nucleus / Cytosol

Table 4: Primer sequences and T_m

Gene	Primer sequence (5'-3')		Melting Temperature (Tm)
GAPDH	5' - TTAGCCCCCCTGGCCAAGG - 3'	FRW	72.2
	5' - CTTACTCCTTGGAGGCCATG - 3'	REV	63.5
Glrx1	5' - GACCCAAGAAATCCTCAGTCA - 3'	FRW	63
	5' - AGATCACTGCATCCGCCTATG - 3'	REV	66.2
Glrx2	5' - CTGCTCTTACTGTTCCATGGC - 3'	FRW	63.7
	5' - GTGAAGCGCATCTTGAAACTGG - 3'	REV	67.9
Txn1	5' - CGTGGTGGACTTCTCTGCTACG - 3'	FRW	68.1
	5' - GGTCGGCATGCATTTGACTTC - 3'	REV	68.7
Txn2	5' - GCTAGAGAAGATGGTCGCC - 3'	FRW	61.6
	5' - TCCTCGTCCTTGATCCCCAC - 3'	REV	68.6
Txnrd1	5' - CAAAATCGGTGAACACATGG - 3'	FRW	63.8
	5' - CACTGTGTTAAATTCGCCCT - 3'	REV	61.5
Txnrd2	5' - GTCCCCTCCCACATCAAAAAAC - 3'	FRW	67.4
	5' - CCACAGGACAGTGTCAAAGG - 3'	REV	63.3
Txnrd3	5' - GTGACGACCTGTTCTCTCTGC - 3'	FRW	64.1
	5' - CACATCTAACCCCAAACCAGCC - 3'	REV	68.4

2.6.4 qPCR reaction

For the qPCR reaction, Real-Time SYBR Green PCR Master Mix in total volume 20 μL/reaction (well) was prepared according to the following recipe (Table 5):

Table 5: Recipe of Real-Time SYBR green PCR Master Mix

Ingredients	Quantities for each reaction (1x)	Quantities for each cDNA (3.5x)
SYBR Select 2x	10 μL	35 μL
Forward Primer	0,4 μL	1,4 μL
Reverse Primer	0,4 μL	1,4 μL
cDNA (50 ng)	0,25 μL	0,875 μL
Sterile dH_2O	8,95 μL	31,33 μL

SYBR® Green is a commonly used fluorescent DNA binding dye which binds to all double-stranded DNA and, due to this fluorescent labeling, the quantification of the amplified DNA molecules can be accomplished. All samples were tested in triplicate (20 μL/ reaction), with master mixes prepared accordingly in order to minimize pipetting errors. A sample without template was used as a control for each primer to exclude contamination and primer-dimer formation. qPCR was performed using a CFX96 Touch Real-Time PCR Detection System (Bio Rad). The cycling procedure is described below:

1. **Initial Heating:** The reaction temperature was increased to 95 °C and the sample was incubated for 3 min.
2. **Cycling:**

a. **Denaturation:** The reaction temperature was increased to 95 °C for 15 sec to ensure that double-stranded DNA (dsDNA) was separated.
b. **Annealing:** The temperature was lowered to 51-53°C for 15 sec to promote primer binding to the template.
c. **Extension:** DNA polymerase extended the sequence-specific primer by incorporating complementary nucleotides to the DNA template at an increased temperature of 72 °C for 30 sec. The reaction progressed for 50 cycles (repeats of steps a, b and c) to ensure effective detection of all genes of interest. As the PCR progresses, more SYBR Green dye binds to the amplicons and hence, the signal intensity increases.

3. **Termination:** For the final step of the procedure, the temperature was lowered to 4 °C until the samples were removed.

The expression of the genes of interest were normalized against the levels of Gapdh expression, in order to determine the up- and down-regulation caused by the experimental conditions.

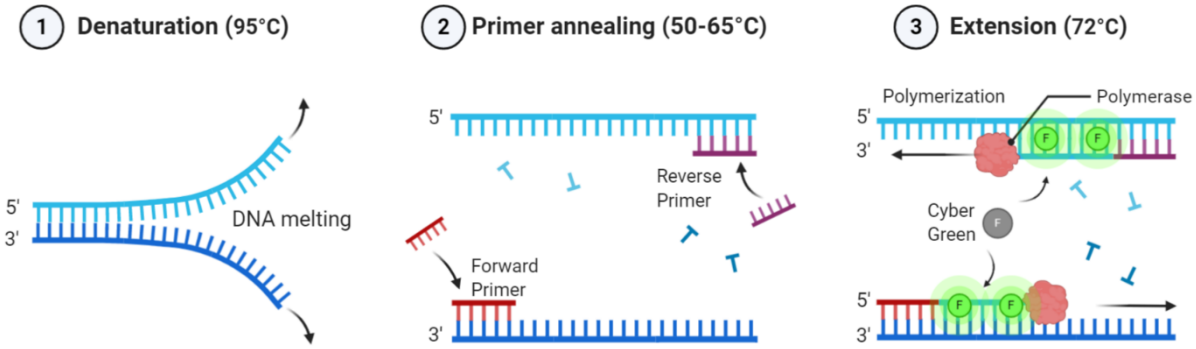

Figure 14: Schematic illustration of qPCR stages.[61]

2.7 Cell Counting

The quantification of the number of cells in the culture, as well as the proper density of the cells for the experimental methods, was determined by a type of counting chamber, the hemocytometer. In more detail, the hemocytometer consists of a glass microscope slide which is separated into two gridded chambers in the middle and a special glass coverslip. [62] A 10 μL sample of the cell suspension was taken using a pipette and then carefully the pipette was placed near the edge of the chamber, allowing the cell suspension to enter the counting chamber by capillary force action. The squares measure 1 mm x 1 mm and are further subdivided into 0.05 mm x 0.05 mm squares, while the chamber is designed in a manner that the special glass

coverslip is placed precisely 0.1 mm above the marked grid (Figure 15). Using a microscope, we focused on the grid lines of the hemocytometer with a 10X objective, then the number of cells counted in the set of 16 squares was manually recorded. This process was repeated by moving the hemocytometer, until all four sets of 16 squares on the hemocytometer have been counted and recorded. The results of the four sets of 16 squares were averaged and multiply by 10,000 to get the number of cells per milliliter in order to establish the concertation of the cells. [63]

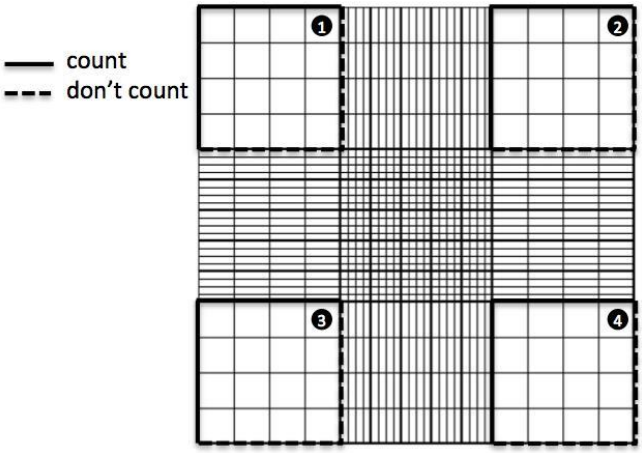

Figure 15: Representative illustration of hemocytometer gridlines, indicating the 4 sets of 16 squares that should be used for counting. [64]

3. Results

3.1 Evaluation of the effect of GO and rGO on the viability and proliferation of MSCs

As a first step, it was essential to evaluate the effects of graphene oxide on the viability and proliferation of MSCs, which were determined after 24h and 48h of exposure to different concentrations of GO and rGO (0-100 μg/mL) using the MTT Viability Assay. MSCs were seeded in 96-well plates using media with or without FBS (+/- FBS). Cells were cultured for 24h and 48h and the protocol for the MTT Viability assay was followed, as described in section 2.3. All results are shown in Figures 16 and 17 and are expressed as the means ± standard deviation of three independent experiments.

MSCs showed reduced viability and proliferation at increased concentrations (50-100 μg/mL) of both GO & rGO, after 24h (Figure 16) and 48 h (Figure 17). On the contrary, treatment with lower quantities of GO/rGO did not seem to effect cell viability and proliferation after 24 h of incubation. Comparing the obtained results between 24h and

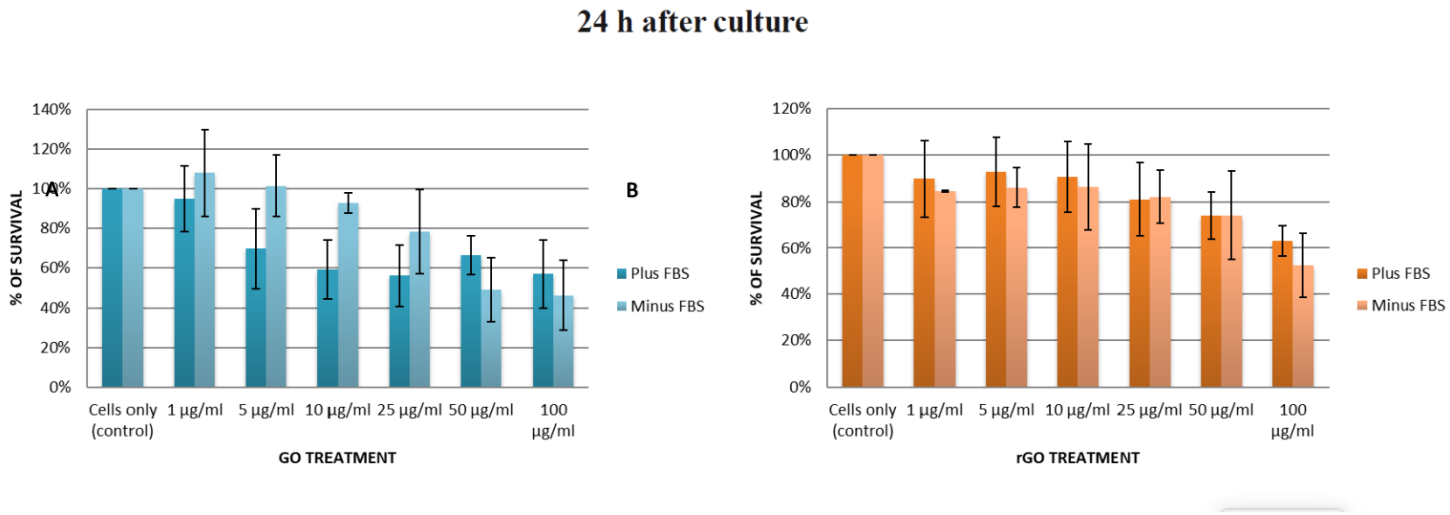

48 h, we discerned higher levels of toxicity after two days of culture in the majority of the samples, irrespective of the medium that was used.

Figure 16: MSCs viability after 24 h of exposure to different concentrations (0-100 μg/mL)of GO (A) and rGO (B) nanocomposites, using plus or minus FBS DMEM (+/- FBS), via MTT assay. Bars indicate standard deviation.

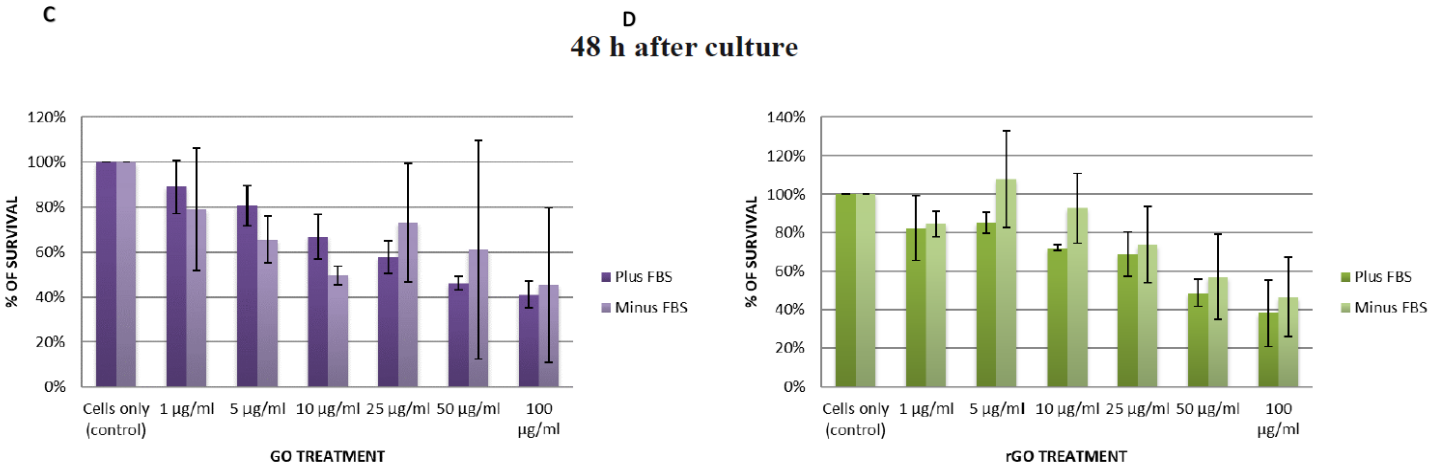

Figure 17: MSCs viability after 48 h of exposure to various concentrations (0-100 μg/mL) of GO (A) and rGO (B) nanocomposites, using plus or minus FBS DMEM (+/- FBS), via MTT assay.

3.2 Validation of the cytotoxic effect of GO & rGO solutions on MSCs

In order to further determine the cytotoxicity of the available solutions, a Live/Dead™ Viability/Cytotoxicity assay was performed. First, MSCs were seeded in 24-well plates using +/- FBS medium and cultured once again for 24h and 48h. In this case, two concentrations of GO and rGO were chosen (10 and 100 μg/mL) as representative examples of lower and higher concentrations of GO and rGO nanocomposites, in order to further explore the toxicity mechanisms of these nanoscale materials on MSCs.

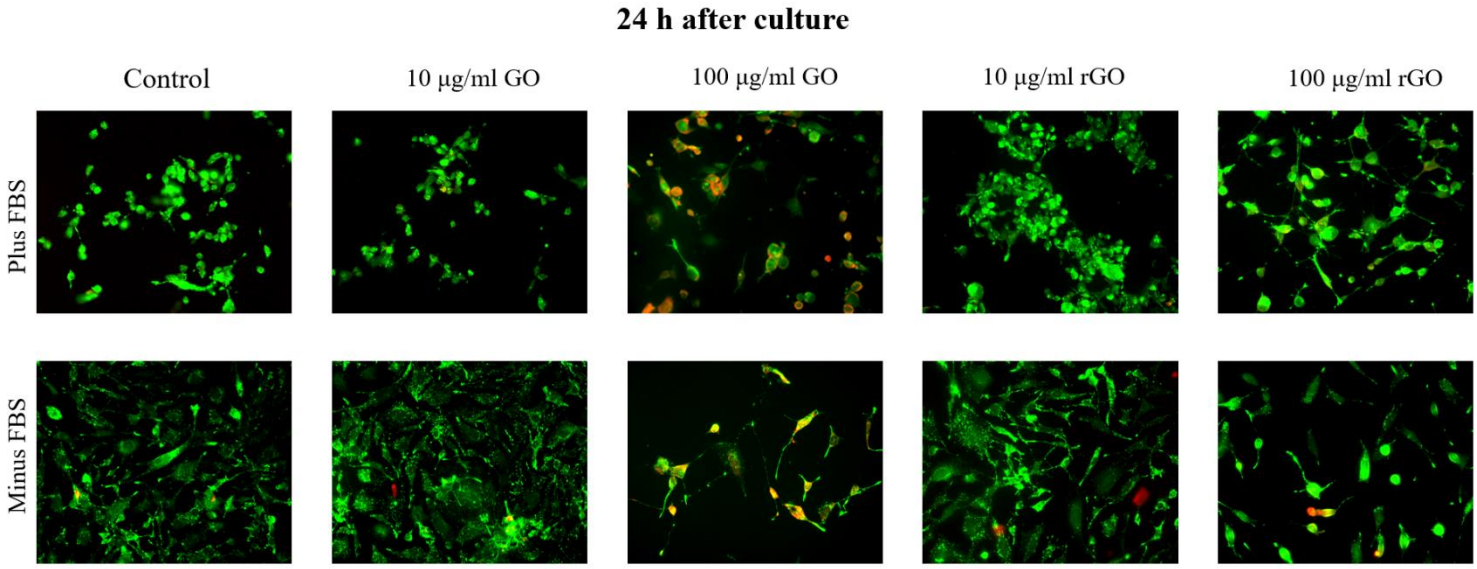

Figure 18: Epifluorescent images of Live/Dead assay after 24 h of culture, for 10 and 100 μg/mL of GO and rGO, using +/- FBS DMEM. Green: calcein indicates living cells, Red: ethidium homodimer-1 (EthD-1) indicates dead cells.

The samples were observed using an epifluorescent microscope and the obtained results were analyzed with Fiji ImageJ. In more detail, cultured cells were fixed with 4% paraformaldehyde (PFA) and nuclei were stained using DAPI. The number of living cells at different time points was analyzed based on fluorescent images of the samples after live/dead cell staining. Cell nuclei were counted by the plugin "Analyze particles" on Fiji ImageJ for the two different time points. Individual experiments were repeated 3 times for each time point and the live/dead ratio was estimated by averaging the results of all three repeats.

Similarly, to the MTT Viability Assay, the results revealed dose- and time-dependent cytotoxicity, with ~ 70% cell death after 24h of exposure to 100 μg/mL GO without the addition of FBS in the culture medium. As can be seen in Figure x the higher the

concentration of the GBM (GO & rGO), the more increased the number of dead cells (cells dyed with red color). Samples containing 100 μg/mL of GO presented the highest levels of cytotoxicity, especially, the samples that were cultured using DMEM without FBS (Figure 18). In addition, higher concentrations exhibited a higher number of cells with morphological defects.

However, it is important to note the difference in cell toxicity between 1 and 2 days of culture. After 48 h, the cellular death rate showed a clearly observable decline, compared with the 24 h results (Figure 19). The results can be seen in the following graphs (Figure 20), which verify the dose-dependent cytotoxicity of graphene oxide (GO) in MSCs, when the latter exposed to higher concentrations, beside its reduced form (rGO), as it shown in Figure 20.

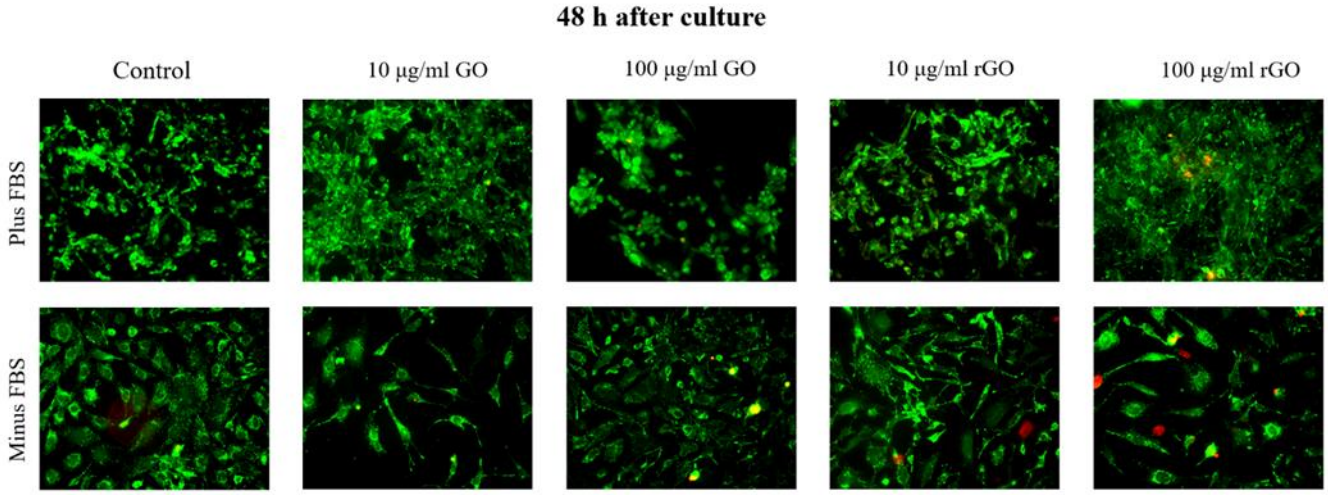

Figure 19: Epifluorescent images of Live/Dead assay after 48 h of culture, for 10 and 100 μg/mL of GO and rGO, using +/- FBS DMEM. Green: calcein-AM indicates living cells, Red: ethidium homodimer-1 (EthD-1) indicates dead cells.

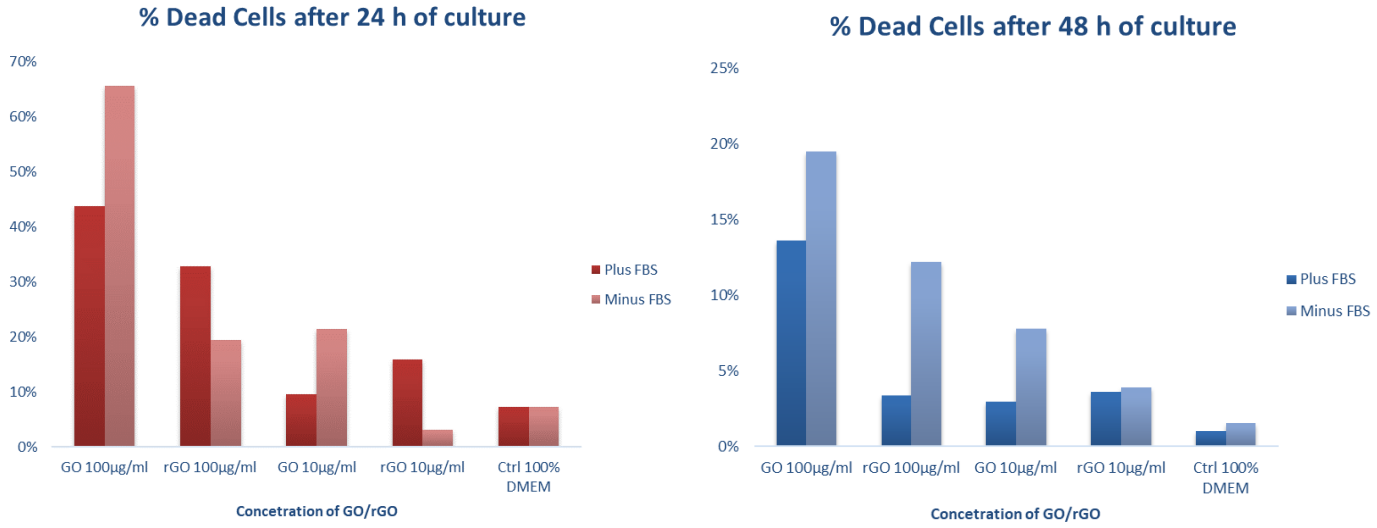

Figure 20: Death rate (percentage) analysis of MSCs for 10 and 100 µg/mL of GO and rGO, using +/- FBS DMEM after 24 (left graph) and 48 h (right graph) of exposure.

3.3 Study of the protein localization & activation of transcription pathways

The subcellular localization of proteins is a significant indicator of processes executed within the different cellular compartments. The accumulation of certain proteins of interest can provide useful information about transcription pathways that are activated through signal transduction, under specific conditions.

As previously mentioned, two major proteins that indicate the activation of transcription pathways under oxidative stress conditions are: Hypoxia inducible factor 1-a (Hif1-a) and Nuclear factor erythroid 2-related factor 2 (Nrf2). Each factor is a core component of a different regulation pathway that is activated when disruption of oxygen homeostasis occurs and mediates the expression of important enzymes of the cellular antioxidant defense system. The import of each regulator into the nucleus denotes the activation of the current pathway. [65]

In order to study the activation of transcription pathways that could potentially be involved in the cellular response to GO and rGO exposure, protein localization was observed through immunocytochemistry. Immunofluorescence (IF) is a type of immunohistochemistry technique that utilizes fluorophores to visualize various cellular antigens such as proteins. To detect protein expression, the biological sample of interest

was fixed using 4% paraformaldehyde (PFA) to prevent protein degradation and simultaneously preserve cellular morphology and properties. This is followed by the incubation of the fixed specimens with a diluted solution of the primary antibody specific to the target protein, which is then detected by a secondary antibody conjugated to a fluorophore (indirect fluorescence). [66]

In this study, the potential activation of the two transcriptional pathways with known expression patterns were investigated using the IF technique. To this end, MSCs were seeded in density of 5x10^4 cells/mL, two groups of experiments were carried out. In group A, samples were exposed to 50 μg/mL GO and rGO for 1h and 4h of incubation, with samples incubated with culture medium plus 10% FBS acting as a negative control and samples treated with same medium and the addition of 200 μg/mL H_2O_2 acting as a positive control (Figures 21-24). In group B, cell cultures were exposed to 5 μg/mL and 50 μg/mL GO and rGO for 24h and 48h (Figures 25-28). In both groups, the expression and the localization (cytoplasmic or nuclear localization) of Hif1-a and Nrf2 were studied through confocal microscopy. The immunolabeling of Hif1-a and Nrf2 was accomplished by a red fluorescence-emitting antibody for the samples in group A, while in group B it was replaced by a green one. The nuclei were stained with DAPI and the actin cytoskeleton staining was carried out with phalloidin 647 for the samples in group A and TRITC phalloidin in group B. The validation of MSCs (group A) proliferation was determined by the proliferation marker Ki-67, which is a protein present in active cells. [67]

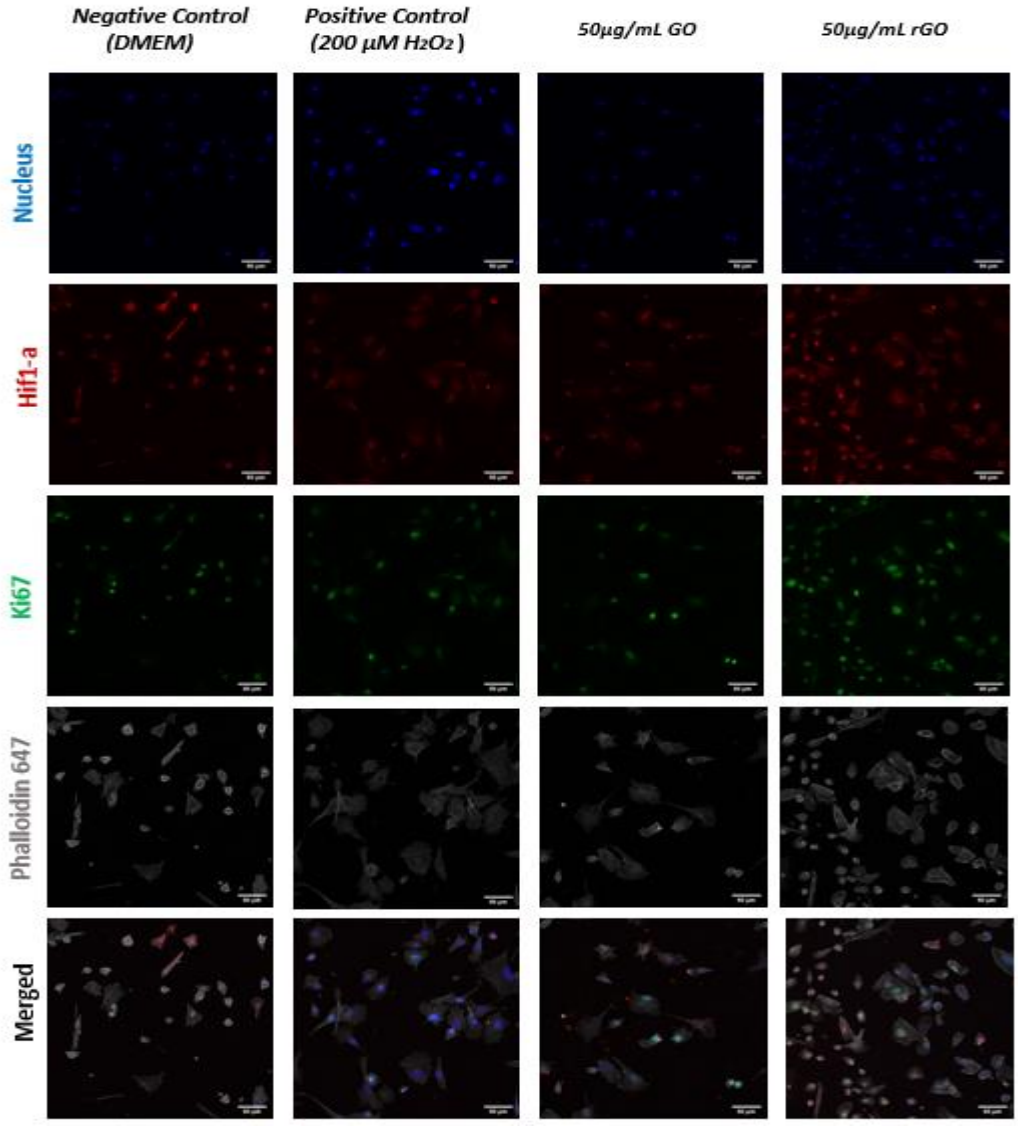

Figure 21: Confocal microscope images of MSCs on glass coverslips, 1 hour after treatment with 0, 50 µg/mL GO/rGO and 200 µM H_2O_2. (Blue: staining of cell nucleus with DAPI, Red: protein of interest; Hypoxia Induced Factor 1-α, Green: Ki67 proliferation marker, Grey: staining of the cell actin with Phalloidin 647).

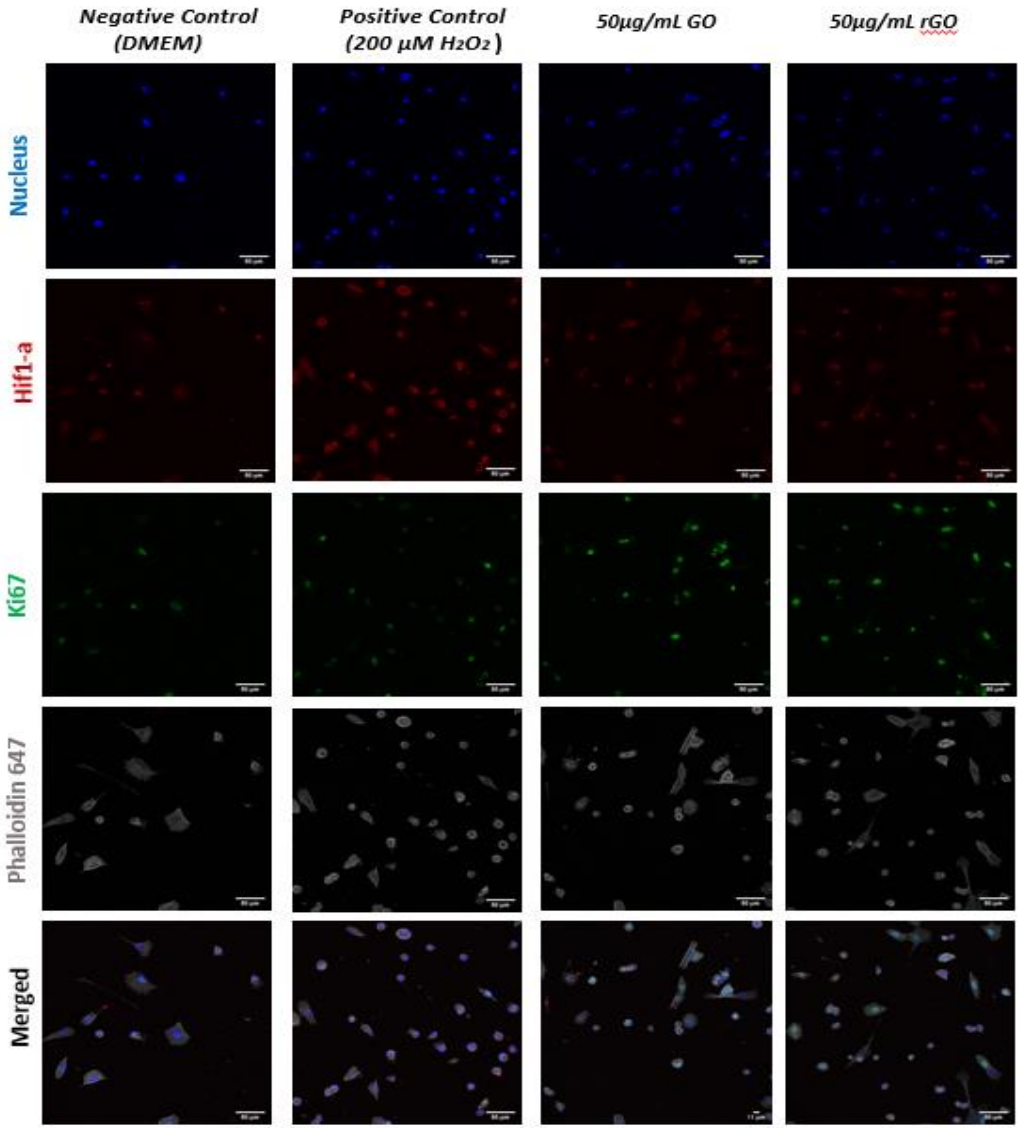

Figure 22: Confocal microscope images of MSCs on glass coverslips, 4 hours after treatment with 0, 50 µg/mL GO/rGO and 200 µM H_2O_2. (Blue: staining of cell nucleus with DAPI, Red: protein of interest; Hypoxia Induced Factor 1-α, Green: Ki67 proliferation marker, Grey: staining of the cell actin with Phalloidin 647).

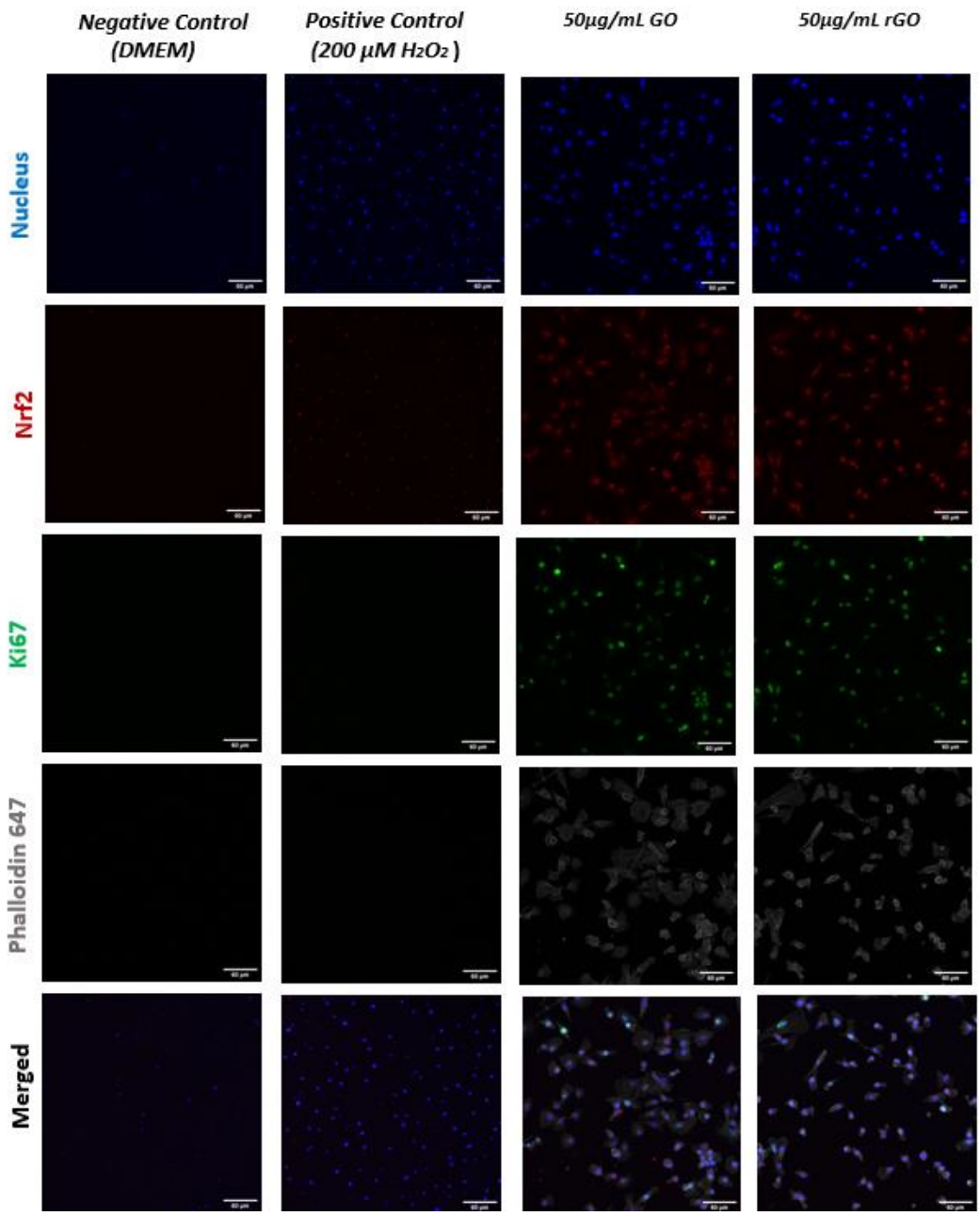

Figure 23: Confocal microscope images of MSCs on glass coverslips, 1 hour after treatment with 0, 50 µg/mL GO/rGO and 200 µM H_2O_2. (Blue: staining of cell nucleus with DAPI, Red: protein of interest; Nuclear erythroid factor 2, Green: Ki67 proliferation marker, Grey: staining of the cell actin with Phalloidin 647).

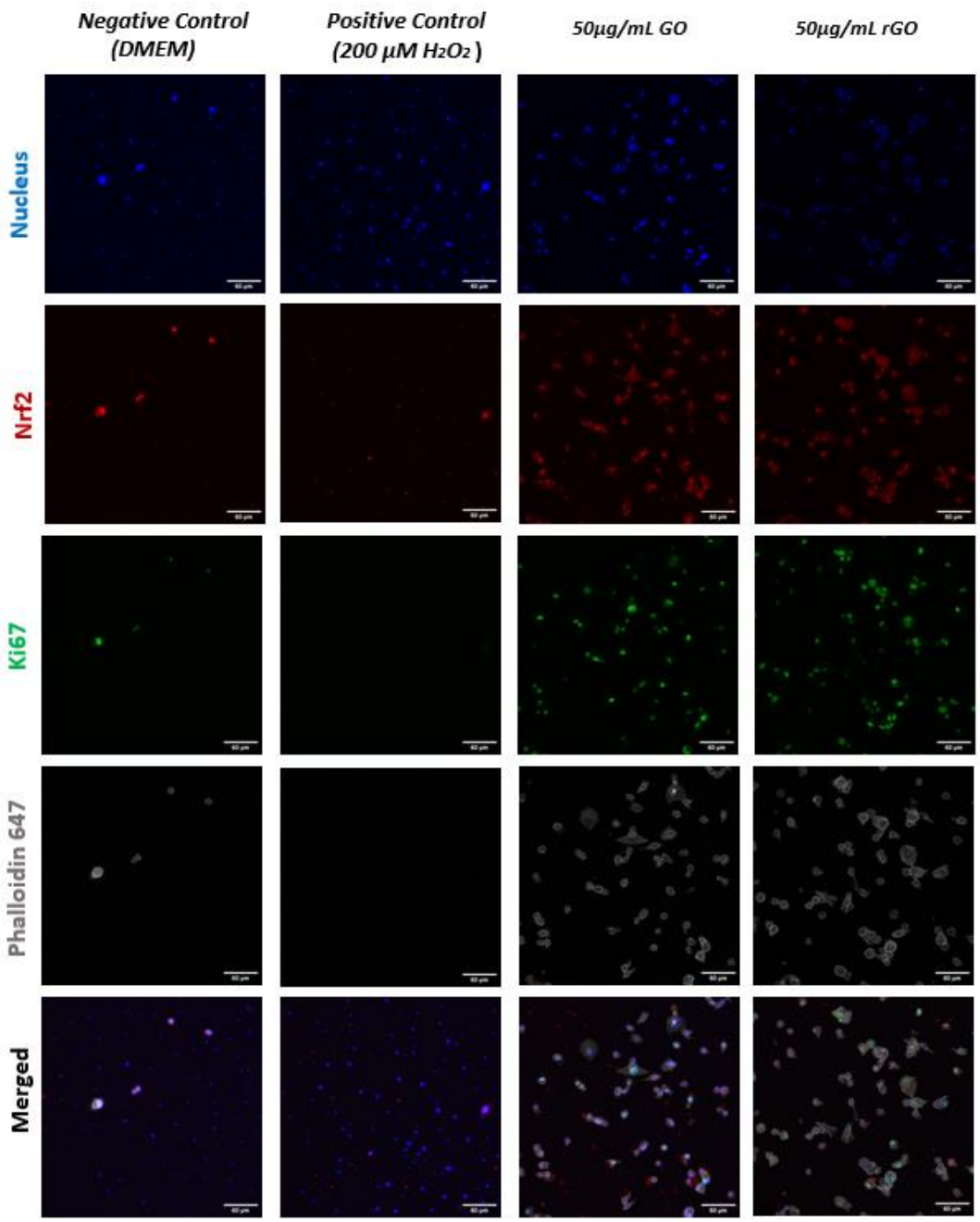

Grey

Figure 24: Confocal microscope images of MSCs on glass coverslips, 1 hour after treatment with 0, 50 µg/mL GO/rGO and 200 µM H2O2. (Blue: staining of cell nucleus with DAPI, Red: protein of interest; Nuclear erythroid factor 2, Green: Ki67 proliferation marker, : staining of the cell actin with Phalloidin 647).

No nuclear accumulation of Hif1-a and Nrf2 was observed after 1h and 4h, while cell growth and proliferation did not seem to be affected by the different treatments. This result indicated that the reaction of interest, which was the potential translocation of the two transcription factors into the nucleus, possibly takes place more than 4h after the initial exposure. As a result, we carried out a series of experiments for 24 h and 48 h (group B).

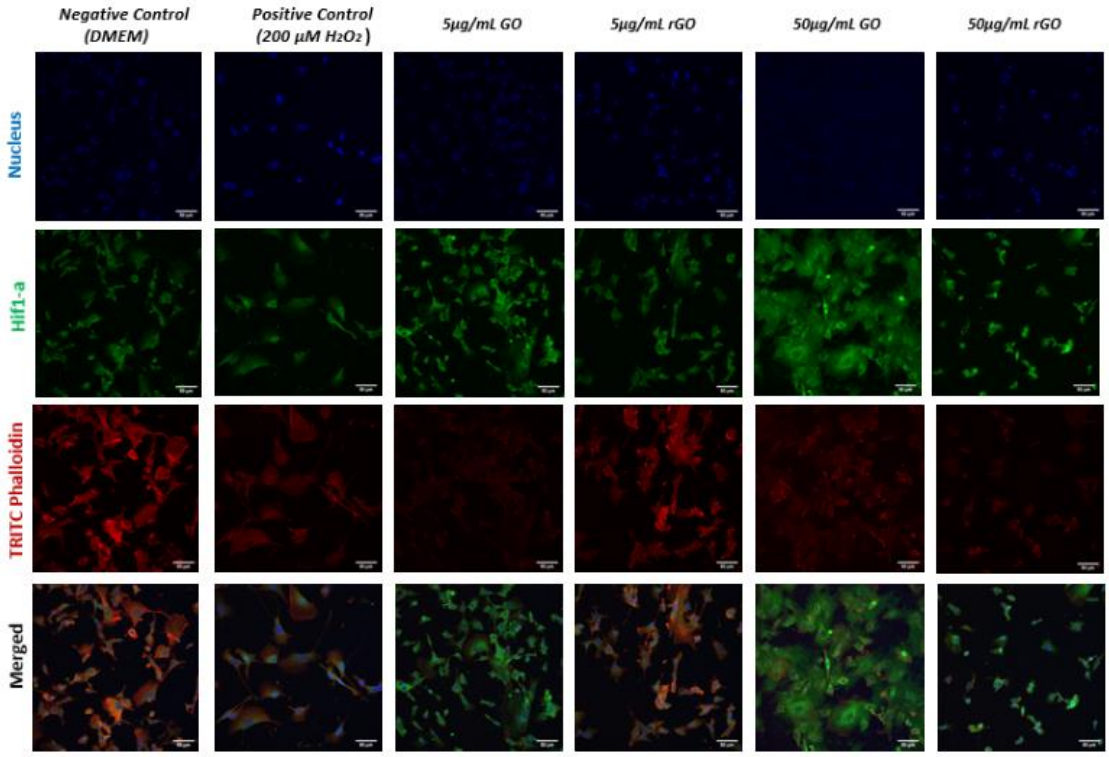

Figure 25: Images of MSCs on glass coverslips, 24 hours after treatment with 0, 5, 50 μg/mL GO/rGO and 200 μM H_2O_2. (Blue: staining of cell nucleus with DAPI, Red: staining of actin filaments with TRITC Phalloidin, Green: Hif1-α).

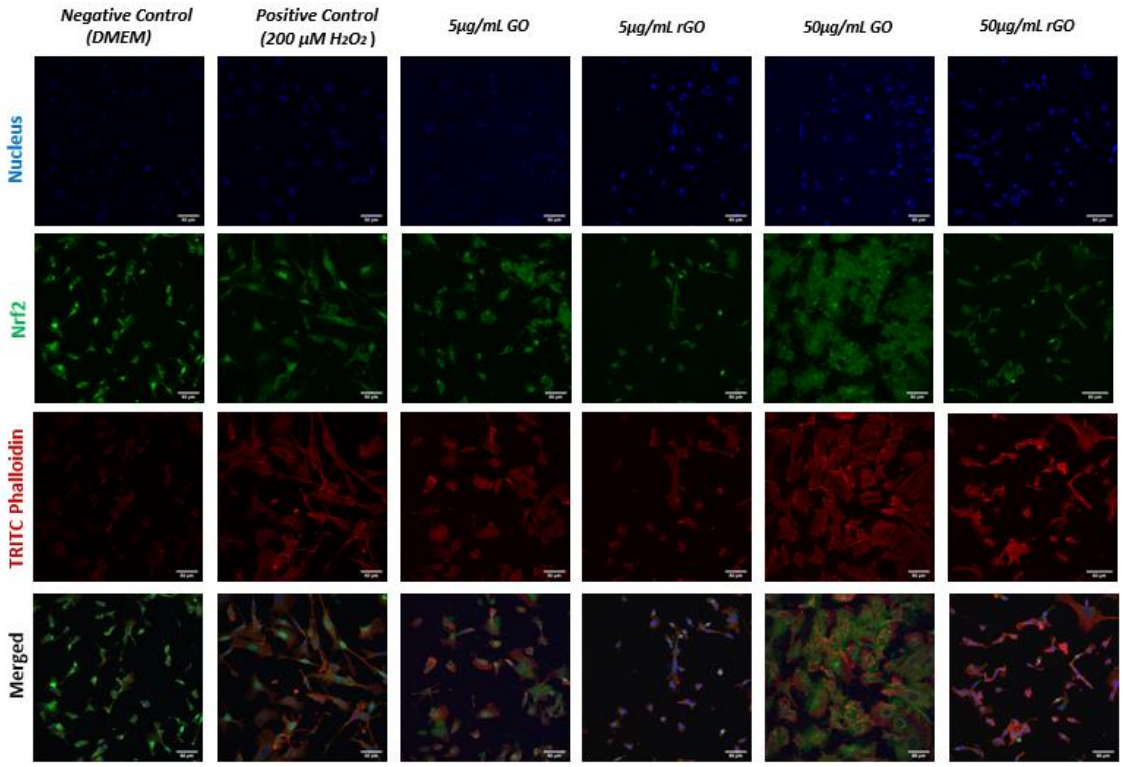

Figure 26: Images of MSCs on glass coverslips, 24 hours after treatment with 0, 5, 50 µg/mL GO/rGO and 200 µM H_2O_2. (Blue: staining of cell nucleus with DAPI, Red: staining of actin filaments with TRITC Phalloidin, Green: Nrf2)

The results obtained after 24h and 48h treatment with GO and rGO exhibited no notable accumulation of either Hif1-a or Nrf2 into the nucleus. Instead, a large proportion of the transcription factors was detected in the cytosol (Figures 25 and 26). Only the cells treated with 50 µg/ml GO demonstrated slightly more intense fluorescence of the Nrf2 protein (Figure 26). These data suggest that the reaction of interest possibly takes place at a different time point between 4 and 24 hours. The image analysis further attested that treatments containing high concentrations of GO aggregated and formed a layer of debris on the surface of the coverslips, as it can be seen in the images of the experimental groups that were exposed to 50 µg/ml GO. The most likely explanation is that these formulated masses were caused by the high density of graphene oxide in the solution.

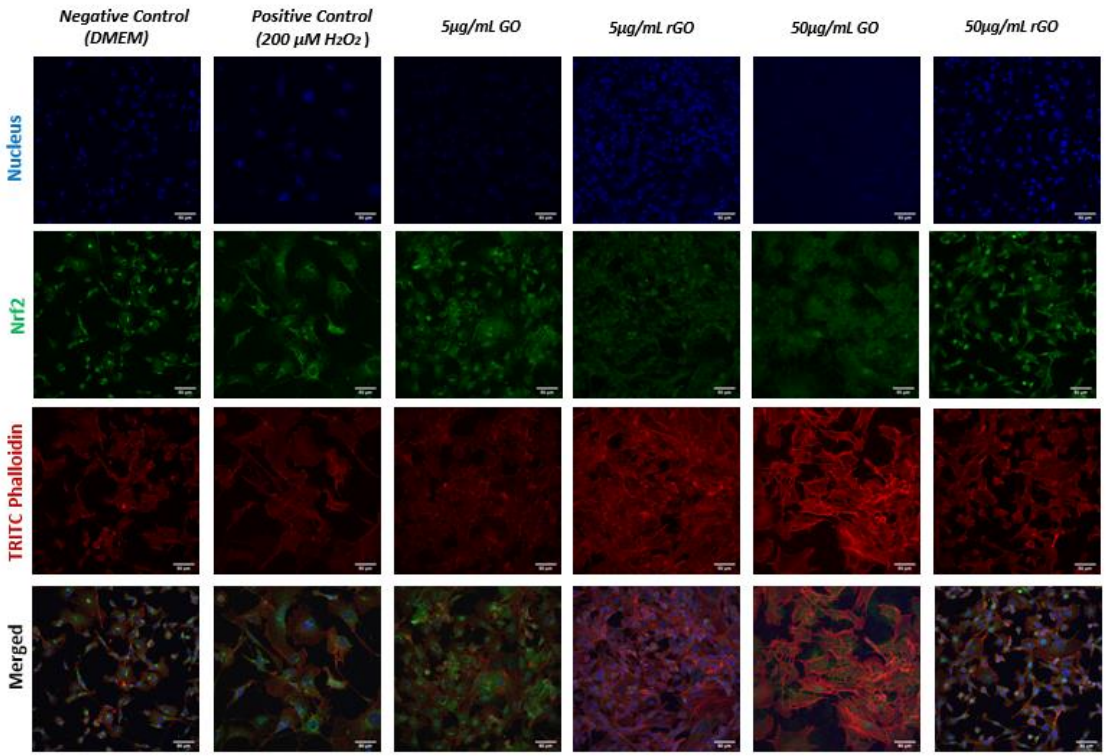

Figure 27: Images of MSCs on glass coverslips, 48 hours after treatment with 0, 5, 50 µg/mL GO/rGO and 200 µM H_2O_2. (Blue: staining of cell nucleus with DAPI, Red: staining of actin filaments with TRITC Phalloidin, Green: Hif1-a).

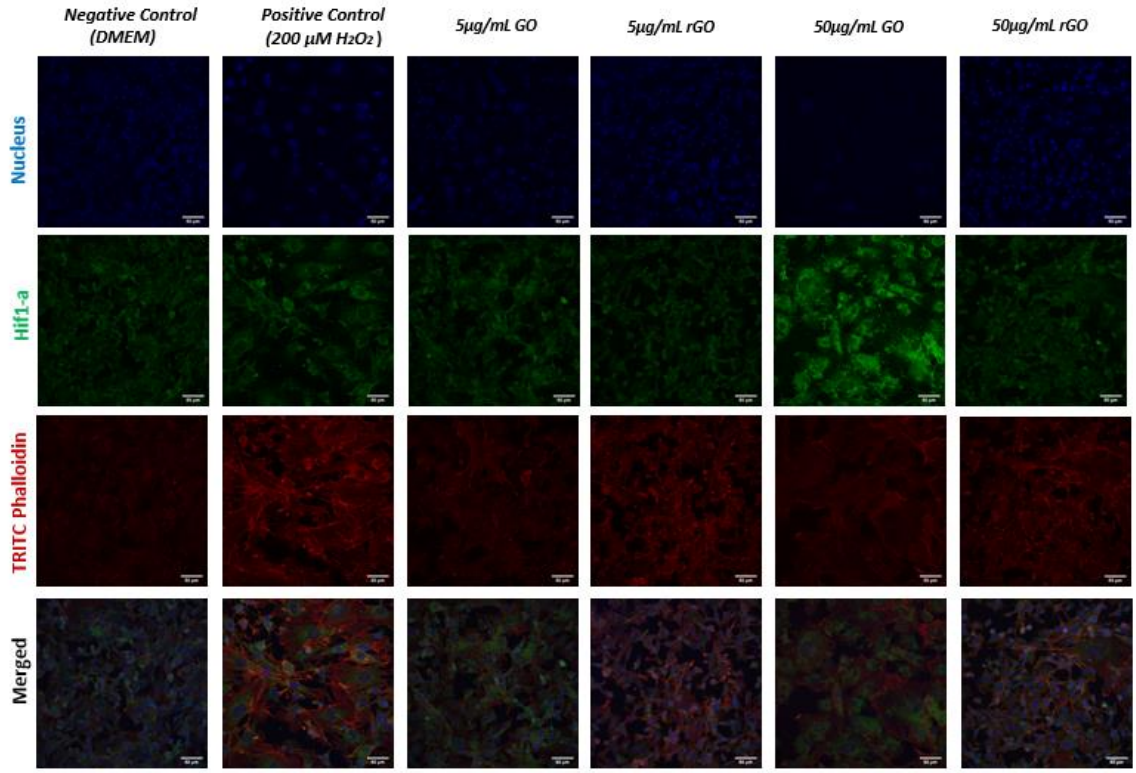

Figure 28: Images of MSCs on glass coverslips, 48 hours after treatment with 0, 5, 50 μg/mL GO/rGO and 200 μM H_2O_2. (Blue: staining of cell nucleus with DAPI, Red: staining of actin filaments with TRITC Phalloidin, Green: Nrf2).

3.4 Gene expression profiling in Mesenchymal Stem Cells (MSCs) measured by qRT-PCR

Oxidative stress can induce the misbalance in pro-oxidant/antioxidant steady state due to generation of increased amount of ROS resulting in cellular damage. [69] Oxidant agents can modulate cellular gene expression and cause damage in cellular components, including DNA, proteins and lipids. Physiologically, the cellular response to ROS involves the activation of a diverse array of protective responses. Therefore, mRNA levels can shed light on the potential activation of signal transduction pathways and determine the genetic regulation correlating with antioxidant responses. [70]

In order to further elucidate the cellular mechanisms activated by the effect of GO and rGO suspensions on MSCs, quantitative real-time polymerase chain reaction (qRT-PCR) was performed. We analysed the mRNA expression levels of 9 target genes related to the Trx and Glrx pathways. Combined with its ease of use, qRT-PCR also provide accuracy, as well as high sensitivity in the verification of gene expression. Nonetheless, there are many variables that can affect the results, including the potential differences of the initial material, enzymatic efficiency and variations between cultures which can impact on the ultimate quantification of cDNA levels. [71] To this end, a specific endogenous expression control relative to a reference group is an important prerequisite for data normalization in order to restore experimental errors. More often, reference genes - also called housekeeping genes - have been widely used for the normalization of the expressed mRNA quantitation. The expression levels of the chosen reference gene should remain constant between the different time points and experimental conditions, for accurate quantification of RNA expression as the cycle thresholds (C_T) of the target genes are compared to those of the reference gene. [72] There are few reference genes which are involved in key, ubiquitous cellular procedures, including β2-microglobulin (B2M), glyceraldehyde 3-phosphate dehydrogenase (GAPDH), β-actin (ACTB), hypoxanthine phosphoribosyl transferase (HPRT) and ribosomal protein L13a (RPL13a). [73]

In this set of experiments, we studied three of the common reference genes mentioned above, Gapdh, Rpl13a and β2m, in order to determine the most appropriate one for target gene transcription in MSCs. The results revealed that the cycle threshold (Cq) values for these genes was quite varied, which indicated that not all three genes had appropriate expression levels to be used as internal control genes (Figure 26). The transcriptional stability analysis of each gene with or without treatment established that GAPDH presented the more consistent expression at various experimental manipulations. Therefore, the levels of gene expression for all experimental conditions tested were normalized against the Gapdh gene.

In our work after 24 h of treatment in DMEM with FBS (+), the cellular exposure to rGO particularly enhanced the expression of the cytosolic Txn1 and mitochondrial Glrx2 genes at a concentration of 50μg/ml. Distinctly, high doses of rGO have induced extremely high upregulation of Txn1 gene expression, as it can be seen in Figures 29 & 30. Furthermore, lower doses of rGO (5μg/ml) also presented corresponding upregulation of the two previously mentioned genes but in a lower scale. Similarly, samples that received the same treatment for 24h and were maintained in DMEM without FBS showed respective up-regulation of the

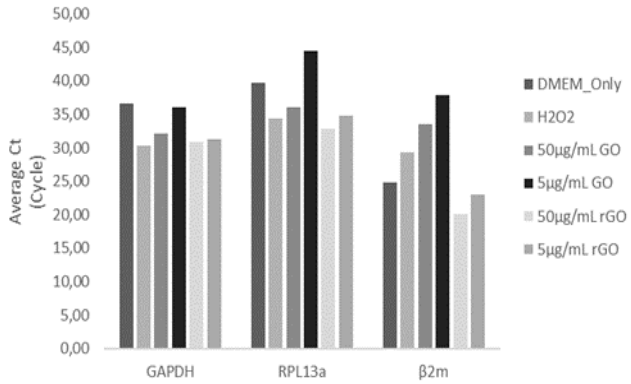

Figure 29: The average cycle threshold (C_q) values of GAPDH, RPl13a and B2M expression in MSCs under different experimental conditions.

Glrx2 and Txn1 genes at a concentration of 5μg/mL rGO. This time, the upregulation of the (mitochondrial) Txnrd2 gene was also observed in the samples containing 50μg/mL GO (Figure 30). In contrast with the previous experiment course, qPCR analysis revealed downregulation of some genes related to the thioredoxin system (Txn/Txnrd genes) including Txn2, Txnrd1, Txnrd3, as well as Glrx2 in all samples.

However, we did not observe any other significant genetic upregulation/downregulation at 24 hours of exposure.

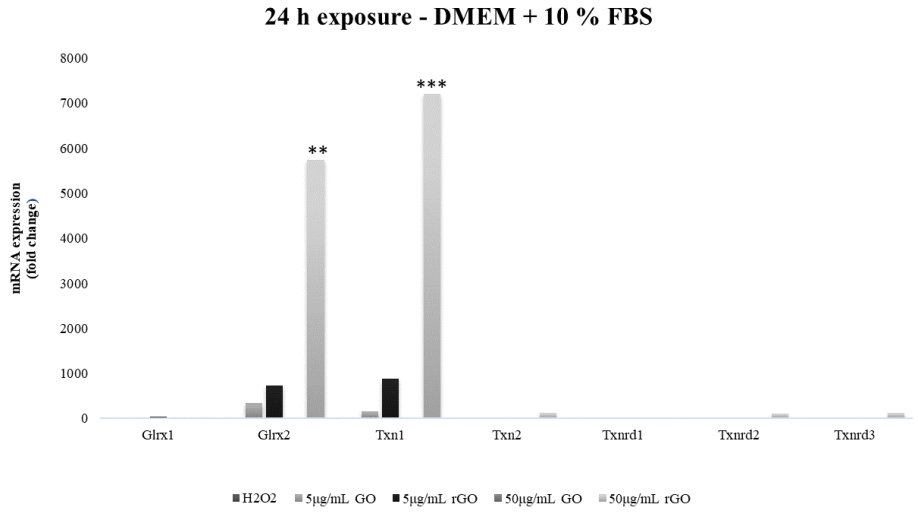

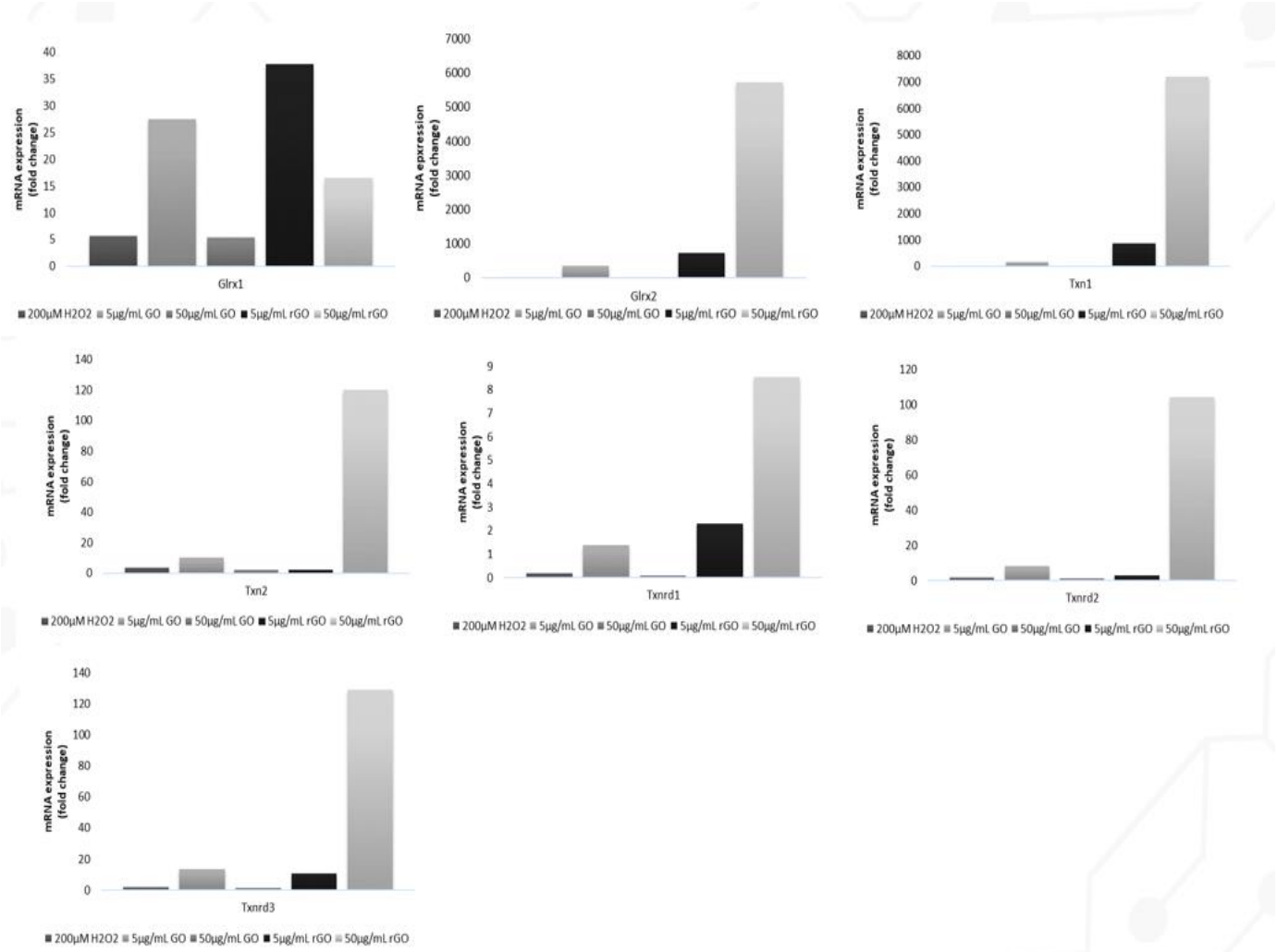

Figure 30: Representative display comparing the expression of the total gene series in MSCs after 24h exposure to GO/rGO, using plus (+) FBS DMEM.

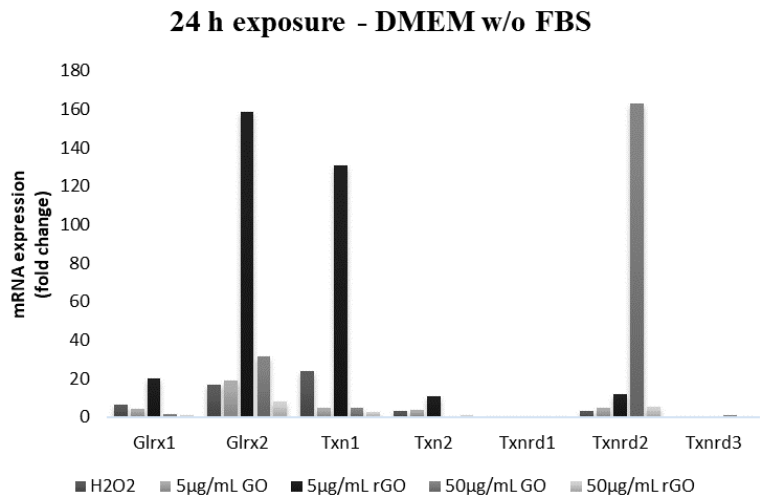

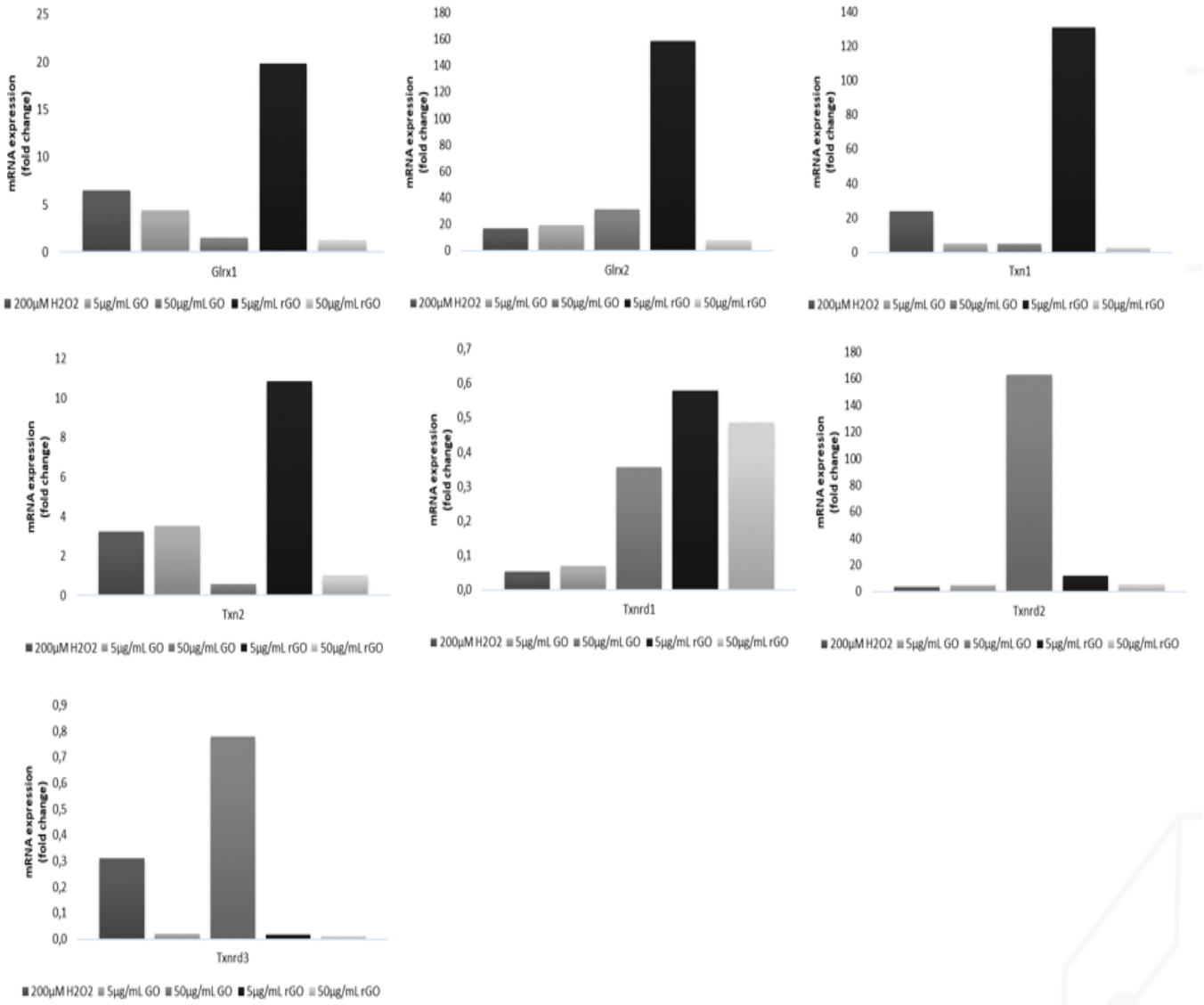

Figure 31: Representative display comparing the expression of the total gene series in MSCs after 24h exposure to GO/rGO, using minus (-) FBS DMEM.

Results after 48 hours of exposure to GO/rGO in DMEM with FBS (+) have indicated a slight increase in the expression of Txnrd1 and Txn2 genes, while for the remaining genes, mRNA levels were reduced by both GO and rGO treatment during the course of the experiment. In contrast, when we used DMEM without (-) FBS, the expression of mitochondrial antioxidant markers Glrx2, Txn2, Txnrd2 and Txnrd3 increased, especially at the concentration doses of 5μg/mL rGO and 50μg/mL GO.

Summarizing the results for the second day after treatment, cells that were exposed to rGO and higher doses of GO are considered to present a transient cellular response to

stress. Moreover, we observed that MSCs that were subjected to GO treatment in minus FBS DMEM were more susceptible to expression changes by GO than the ones that were maintained in plus FBS DMEM, suggesting that FBS supplementation may act in a protective way and be involved in the inhibition of genetic changes to graphene oxide. Notably, all experiments from both time points have indicated dose- and time-dependent changes in genetic expression after GO and rGO treatment.

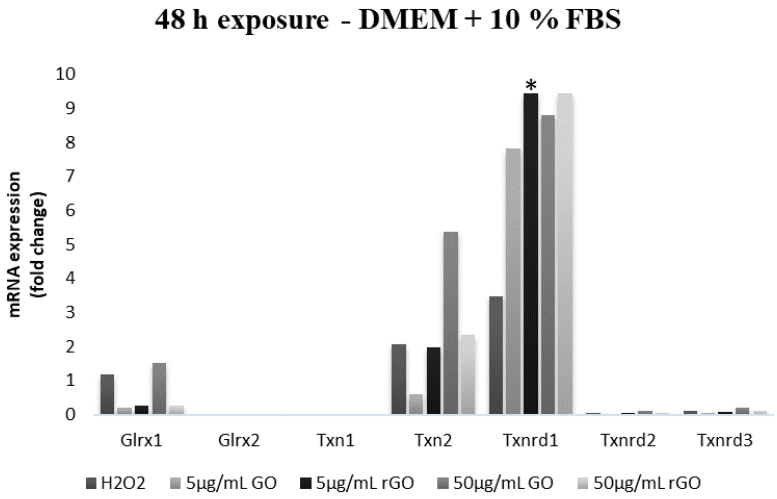

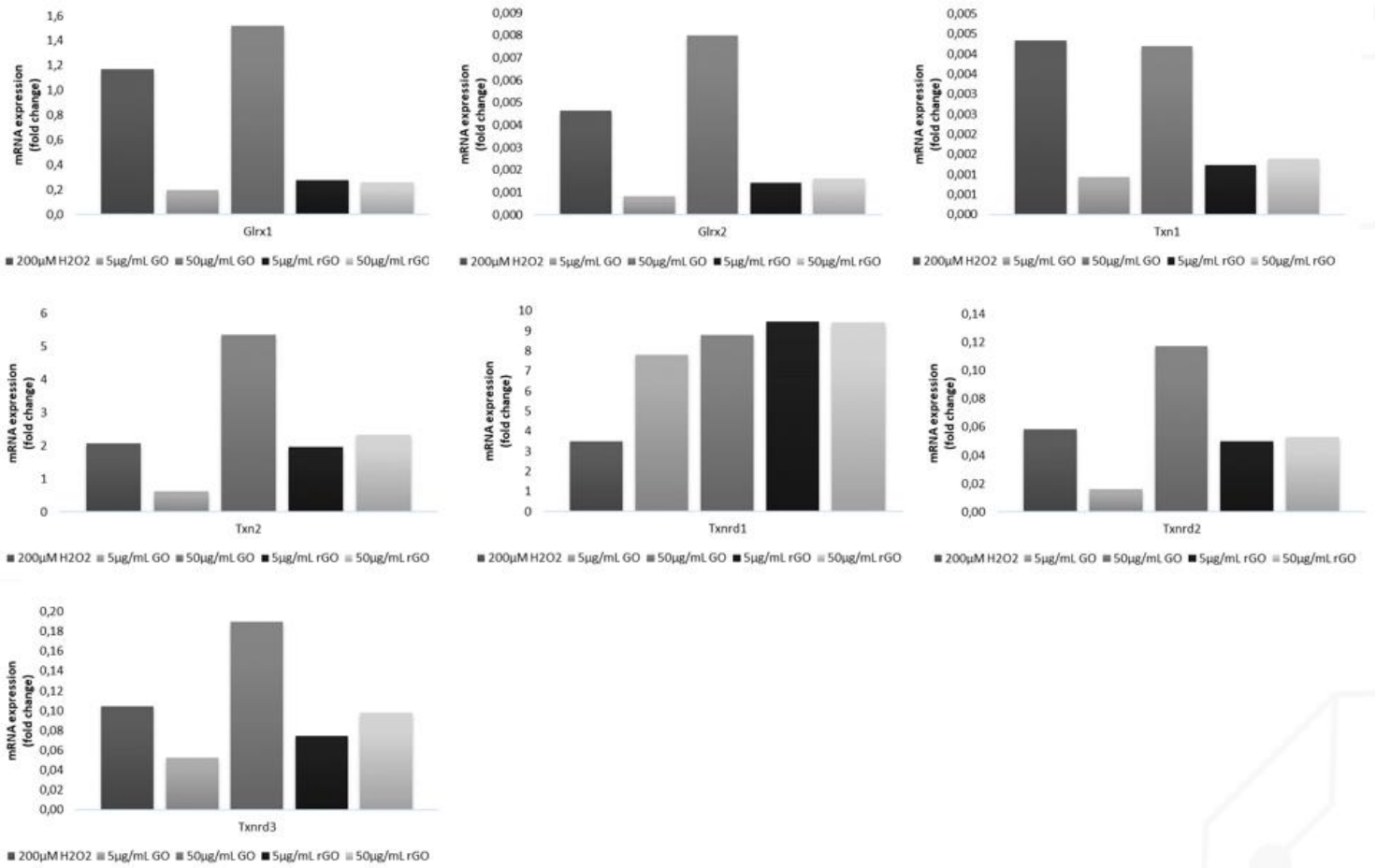

Figure 32: Representative display comparing the expression of the total gene series in MSCs after 48 h exposure to GO/rGO, using plus (+) FBS DMEM.

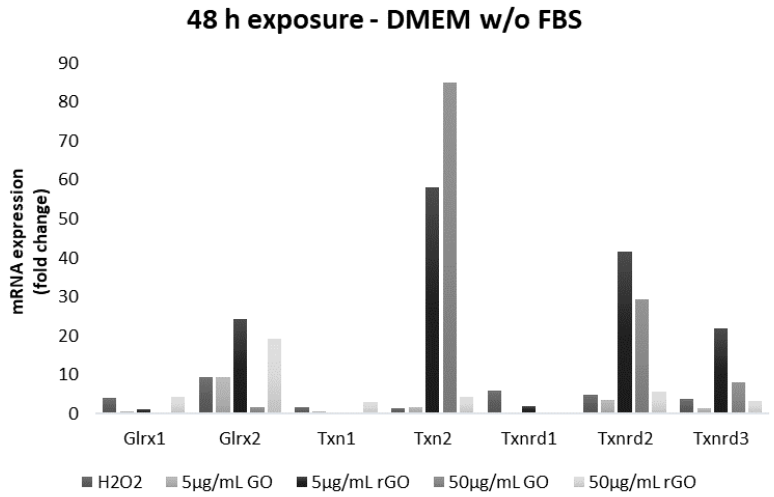

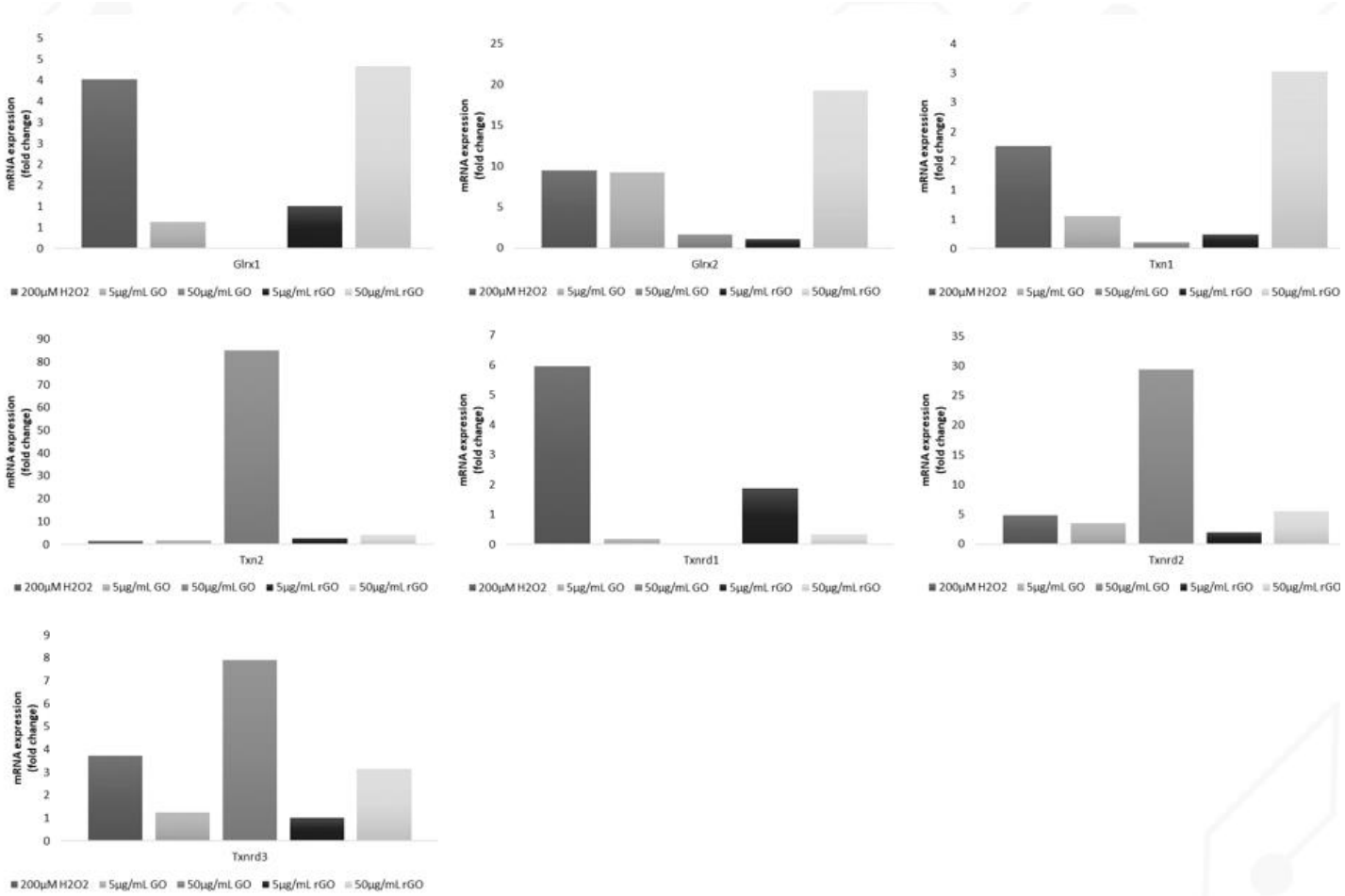

Figure 33: Representative display comparing the expression of the total gene series in MSCs after 48 h exposure to GO/rGO, using DMEM without (-) FBS.

4. Discussion

There is rapidly growing interest in the use of graphene family nanomaterials (GFNs) as potential candidates in a large number of tissue engineering applications, due to their exceptional features and properties. More specifically, graphene-derived GO and rGO are considered two of the most promising nanoplatforms, capable of promoting the regenerative potential and restore the functional activities of a wide range of tissues and organs. Therefore, the underlying mechanisms that GFNs activate, along with their toxic potentials, needed to be further evaluated. [68]

The present thesis aimed to determine the effects of graphene oxide and its reduced substrate rGO on the oxidative response in mesenchymal stem cells (MSCs). In more

detail, we elucidated the *in vitro* toxicity caused after 24 and 48 hours of exposure to treatment with different concentrations/doses of GO and rGO, using DMEM with or without FBS supplement (10%). Several experiments have been performed in order to assess the impact of the graphene derivatives on the proliferation/viability, cytotoxicity, localization of key transcriptional factors and finally, gene expression on MSCs.

The MTT experiments were conducted to evaluate the adverse effect of the two graphene-based nanomaterials in cell culture, which revealed dose-dependent toxicity of GO and rGO on the viability and the proliferation of MSCs, with GO presenting higher impact than rGO at higher doses. MSCs that were exposed to either GO or rGO at the concentration of 1 and 10 μg/mL, regardless of the presence or absence of FBS, have shown similar behaviors to the untreated control samples. In contrast, concentrations beyond 25 μg/mL seemed to have stronger impact on MSCs that were treated with GO/rGO in minus FBS DMEM. After 48 h, the survival rate of the cells was decreased especially in the samples that were exposed to GO treatment compared to 24 h, indicating time-dependent toxicity. The cellular damage was correlated with the oxidation state of these carbon nanomaterials. Our data analysis after 48 h of exposure to GO in DMEM without FBS has presented a significant variation in the cytotoxicity results of the particular samples as it can be seen from the error bars in figure 16. This could be due to the high complexity of the biological systems; it is possible that living organisms; like cells, might slightly vary in the way they react even at the exact same conditions. A number of studies have demonstrated that graphene oxide and reduced GO exhibit toxicity in a concentration- and time-dependent manner to various cell types. *Wang and co-workers* have reported concentration dependency of GO cytotoxicity in human lung fibroblast (HLF) cells, the induced cytotoxicity was assessed by the MTT assay and the trypan blue staining. The results have also presented a decrease in the metabolic activity of fibroblasts with GO and at higher concentrations of chemically-reduced GO, which became more intense within a prolonged treating time.[69] Furthermore, *Das et. al* ascertain the concentration- and time- dependent reduction in cell viability after 24 h and 48h of exposure to GO and rGO, in human umbilical vein endothelial cells (HUVEC). Their results also showed that rGO is less toxic than GO in various cell cultures; they were able to assess theirr statement by the MTT assays that they carried out in both human keratinocytic cell line (HaCaT) and human osteosarcoma cells (MG63). [70] We speculated that the high oxygen content,

better water solubility, and active surfaces are the significant factors responsible for higher toxicity of GO.

To further confirm our results, we performed a Live/Dead assay where the cytotoxicity of two GNFs was evaluated according to the number of live and dead cells. Our findings were consistent with the MTT results, as the higher the dose of the nanomaterial, the greater the number of dead cells and thus, there is increased cytotoxicity. Samples that were maintained in DMEM with FBS seemed to be less affected by GO/rGO toxicity compared to the ones where DMEM without FBS was used. Once again, the data have revealed rGO did not decrease cell viability at the concentration of 10 μg/ml. However, exposure to GO and rGO have caused dose-dependent cytotoxicity in MSCs in the concentration range of 100 μg/mL, which have become more intense in presence of minus FBS DMEM. In contrast with our previous findings, the obtained data after 48 h have shown a drop in cell death. Other studies also confirm that due to the fact that GO contains more reactive functional groups (-OH, -COOH, C-O as epoxy and alkoxy) and therefore the interaction with biological macromolecules is endowed, GO has greater potential to toxicity than its RGO derivative.[70] These results suggested that rGO nanocomposites have shown better biocompatibility toward MSCs than GO.

The staining experiments that were performed in the presence of the GO and rGO treatment in order to elucidate the localization of the two transcription factors: Nrf2 and Hif1-α, during oxidative stress conditions, were unable to lead to a conclusion concerning the nucleus import for the selective timepoints, at any of the conditions assayed. More specifically, the experimental set up that was used could not detect the sustained activation of the particular key proteins. The individual experiments that were conducted for short-term (1-4 h) and long-term (24-48 h) exposure to GO/rGO treatment report that the reaction of interest possibly takes place at a timepoint between 4 h and 24 h. Interestingly, at the concentration of 50 μg/mL GO we observed a more intense fluorescence of the Nrf2 transcription factor, which support our previous statement about the potential timepoint range of the reaction of interest. *Bak et al.* demonstrated that rGO was associated with the activation of Nrf2/ARE pathway in HepG2-C8 and HepG2 cells, respectively. Their findings revealed a 230% increase in the subcellular translocation of Nrf2 into the nucleus, after 2 h of treatment with 50 μg/mL of rGO. [71] *Tang et al.* confirm the nuclear accumulation of Nrf2 in MG-63 cells after exposure to treatment with 25 μg/ml GO for 2 h, however K_7M_2 cells did not

display the same behavior.[72] Furthermore, *Krick et al.* assessed the induced HIF-1α translocation from the cytoplasm to the nuclei in ATII and A549 cells by immunocytochemistry after 24 h and 48 h under hypoxic conditions. The results showed nuclear fluorescence in both cell types after 24 h of exposure.[73] The differences between these studies, in terms of the cell line used as well as the timing of treatment, may be sufficient to explain these contrasting results. Nonetheless, the different DMEMs did not seem to affect the subcellular distribution of Nrf2 and HIF-1α.

Overall, gene expression plays significant role in cellular homeostasis. Oxidative stress can lead to deregulation of gene expression, causing DNA damage. Therefore, to verify our findings in this study, we measured the expression of 7 Txn- and Glrx systems related genes, which tightly control the cellular redox state, by qRT-PCR. The specific genes are induced upon activation of the key antioxidant defense of the cell; thus, the mRNA level patterns reflect mechanisms involved in adaptation to oxidative conditions. Upon exposure to 50μg/ml of rGO after 24 h in DMEM with FBS (+), the cytosolic Txn1 and mitochondrial Glrx2 genes were robustly upregulated, these results are in agreement with the fact that thioredoxin system is the master regulator of the cellular redox-milieu. Generally, 24 h exposure to rGO using either DMEMs led to increased levels of mRNA expression of those genes at both concertation-doses though in a lower scale. At the same timepoint, GO treatment only induced the upregulation of (mitochondrial) Txnrd2 50μg/ml, while genes related with Txn system were downregulated. We also observed increased levels of the respective reductase Txnrd1 after 48 hours of exposure to GO/rGO in DMEM with FBS (+) as well as Txn2 (mitochondrial) while the Txn1 and Glrx2 were downregulated. The relative changes in the level of the previously mentioned genes indicated the activation of the main ROS scavengers. Regarding the increased levels of mitochondrial Glrx2, Txn2, Txnrd2 and Txnrd3 in response to concentration-doses of 50μg/mL GO using DMEM without FBS, we proposed that GO has more impact on cells treated with the particular DMEM compared to the ones that were maintained in plus FBS DMEM. We assumed that the observed impact of GO on gene expression in absence of FBS supplement, in contrast with rGO, is the result of its unique chemo-physical properties and the functional groups on its surface. The FBS supplementation seemed to attenuated the genetic changes to graphene oxide and thus, reinforce the antioxidant cellular action. This

deregulation of known oxidative stress markers, with respect to GO especially in DMEM without FBS, is in accordance with our MTT and Live/Dead assay. Furthermore, *Duch and coworkers* report that it is possible to reduce the toxic effect of the GO for their usage in tissue engineering applications by controlling the oxidation of graphene and limiting the functional group density on the GO surface.[74] A wide number of studies have shown that functional group density on the surface of the graphene oxide and its reduced form significantly affect cytotoxicity, suggesting that the reduction of functional group density accumulated on GO surface could alleviate the toxicity.[70] To this end, *Szmidt et al.* proposed GO could evoke mitochondrial dysfunction that leads to the down-regulation of the expression of nuclear genes encoding mitochondrial proteins. Another study demonstrates chicken embryo cells treated with different types of graphene, including GO, and rGO have presented disrupted mitochondria, also GBM cells grown *in ovo* (in the egg) and treated with GO and rGO had degraded mitochondria. [75] These observations indicate that all individual experiments for both 24 h and 48 h of exposure to GO/rGOspecifically induce mRNA expression in a dose-dependent manner in response to oxidative stress. Hence, the obtained results indicate that both the thioredoxin and glutaredoxin systems play an important role in cellular resistance to oxidative stress.

5. Conclusion

Collectively, this study suggests that graphene oxide and reduced graphene oxide hold great promise for use in several tissue engineering applications, however it is essential that their potential impact on both health and the environment is properly assessed. Our experiments have revealed dose- and time- dependent toxicity of GO and rGO in MSCs, with rGO presenting less cytotoxic effect than GO. As for the two key transcriptional factors of oxidative stress that were studied, we suggest that the potential translocation of Hif1-α and Nrf2 into the nucleus takes place at a different time point between 4 and 24 hours. We demonstrate that mRNA expression of genes involved in redox cellular system were affected by GO and rGO treatment. Finally, our data suggest a potential protective role in FBS supplement in the DMEM which contributes in the inhibition of genetic changes to graphene oxide. Further studies need to be conducted in order to further evaluate the underlying effect of GO and rGO on MSCs.

References

[1] Meyer, U. (2009). **The History of Tissue Engineering and Regenerative Medicine in Perspective.**

[2] Vacanti, J., Vacanti, C. (2000). Chapter 1. **The History and Scope of Tissue Engineering.** Principles of Tissue Engineering: Fourth Edition.

[3] Fengxuan, H., Jiayuan, W., Luguang, D., Yuanbin, H., et al. (2020). **Tissue Engineering and Regenerative Medicine: Achievements, Future, and Sustainability in Asia.** Frontiers in Bioengineering and Biotechnology, vol. 8

[4] Dhandayuthapani, B., Yoshida, Y., Maekawa, T., Kumar, D. S. **Polymeric Scaffolds in Tissue Engineering Application: A Review,** International Journal of Polymer Science, vol. 2011

[5] Asadian, M., Chan, Norouzi, Grande, S., et al. (2020). **Fabrication and Plasma Modification of Nanofibrous Tissue Engineering Scaffolds.** Nanomaterials

[6] Ayala, A., Muñoz, M. F., & Argüelles, S. (2014). **Lipid Peroxidation: Production, Metabolism, and Signalling Mechanisms of Malondialdehyde and 4-Hydroxy-2-Nonenal. Oxidative Medicine and Cellular Longevity**, 1–31.

[7] Nordberg, J., & Arnér, E. S. (2001). **Reactive oxygen species, antioxidants, and the mammalian thioredoxin system.** Free radical biology & medicine, 31(11), 1287–1312.

[8] Akhigbe, R., Ajayi, A. (2021). **The impact of reactive oxygen species in the development of cardiometabolic disorders: a review.** Lipids in Health and Disease. 20.

[9] Aon, M. A., Stanley, B. A., Sivakumaran, et al. (2012). **Glutathione/thioredoxin systems modulate mitochondrial H2O2 emission: an experimental-computational study.** The Journal of general physiology, *139*(6), 479–491.

[10] **Reactive Oxygen Species (ROS).** AAT Bioquest

[11] Sharifi-Rad, M., Anil Kumar, N. V., Zucca, P. et al. (2020). **Lifestyle, Oxidative Stress, and Antioxidants: Back and Forth in the Pathophysiology of Chronic Diseases**. Frontiers in physiology, 11, 694.

[12] Sullivan, L.B., Chandel, N.S. (2014) **Mitochondrial reactive oxygen species and cancer.** Cancer Metab 2**,** 17

[13] Miyamoto, Y., Koh, Y. H., Park, Y. S., et al. (2003). **Oxidative stress caused by inactivation of glutathione peroxidase and adaptive responses.** Biological Chemistry, 384(4)

[14] Holmgren A. (1989). **Thioredoxin and glutaredoxin systems.** The Journal of biological chemistry, 264(24), 13963–13966.

[15] Balsera, M., & Buchanan, B. B. (2019). **Evolution of the thioredoxin system as a step enabling adaptation to oxidative stress.** Free radical biology & medicine, *140*, 28–35.

[16] Lanci, S.A. (2016). **An Investigation of the Succination of the Selenoproteins Thioredoxin Reductase and Glutathione Peroxidase.**

[17] Vlamis-Gardikas, A., Holmgren, A. (2002). **Thioredoxin and glutaredoxin isoforms.** Methods in enzymology, 347, 286–296. https://doi.org/10.1016/s0076-6879(02)47028-0

[18] Fan, Q., Zhang, Y., Liu, Y., et al. (2016). **Glutaredoxin Desensitizes Lens to Oxidative Stress by Connecting and Integrating Specific Signaling and Transcriptional Regulation for Antioxidant Response.** Cellular physiology and biochemistry international journal of experimental cellular physiology, biochemistry, and pharmacology, 39(5), 1813–1826.

[19] Musaogullari, A., & Chai, Y. C. (2020). **Redox Regulation by Protein S-Glutathionylation: From Molecular Mechanisms to Implications in Health and Disease.** International journal of molecular sciences, 21(21), 8113.

[20] Kazzaz, J. A., Xu, J., Palaia, T. et al. (1996). **Cellular oxygen toxicity.** Oxidant injury without apoptosis. The Journal of biological chemistry, 271(25), 15182–15186.

[21] Lee, J. W., Ko, J., Ju, C., & Eltzschig, H. K. (2019). **Hypoxia signaling in human diseases and therapeutic targets.** Experimental & molecular medicine, 51(6), 1–13

[22] Semenza G. L. (2001). **HIF-1 and mechanisms of hypoxia sensing.** Current opinion in cell biology, 13(2), 167–171.

[23] Wheaton, W. W., & Chandel, N. S. (2011). **Hypoxia. 2. Hypoxia regulates cellular metabolism.** American journal of physiology. Cell physiology, 300(3), C385–C393.

[24] Zaher, T. E., Miller, E. J., Morrow, D. M. P., et al. (2007). **Hyperoxia-induced signal transduction pathways in pulmonary epithelial cells.** Free Radical Biology and Medicine, 42(7), 897–908.

[25] Xuefei, Y., Xinyi, Z., Qing, C., et al. (2021). **Effects of Hyperoxia on Mitochondrial Homeostasis: Are Mitochondria the Hub for Bronchopulmonary Dysplasia?.** Frontiers in cell and developmental biology, 9, 642717.

[26] Ma Q. (2013). **Role of nrf2 in oxidative stress and toxicity.** Annual review of pharmacology and toxicology, 53, 401–426.

[27] Zhang, Z., Zhou, S., Jiang, X., et al. (2015). **The role of the Nrf2/Keap1 pathway in obesity and metabolic syndrome.** Reviews in endocrine & metabolic disorders, 16(1), 35–45.

[28] Maleki M, Zarezadeh R, Nouri M, et al. **Graphene Oxide: A Promising Material for Regenerative Medicine and Tissue Engineering.** Biomolecular Concepts. 2020 Dec;11(1):182-200

[29] Han, S., Sun, J., He, S., Tang, M., & Chai, R. (2019). **The application of graphene-based biomaterials in biomedicine**. American journal of translational research, 11(6), 3246–3260.

[30] Aydin, T., Gurcan, C., Taheri, H., & Yilmazer, A. (2018**). Graphene Based Materials in Neural Tissue Regeneration.** Advances in experimental medicine and biology, 1107, 129–142.

[31] Bhattacharjee, S., Joshi, R. K., Chughtai, A. A., Macintyre, C. R., **Graphene Modified Multifunctional Personal Protective Clothing.** Adv. Mater. Interfaces 2019, 6, 1900622

[32] Xue, W., Du, J., Li, Q., et al. (2022). **Preparation, Properties, and Application of Graphene-Based Materials in Tissue Engineering Scaffolds.** Tissue engineering. Part B, Reviews, 10.1089/ten.TEB.2021.0127. Advance online publication

[33] Shin, S. R., Li, Y. C., Jang, H. L., Khoshakhlagh, P., et al. (2016). **Graphene-based materials for tissue engineering.** Advanced drug delivery reviews, 105(Pt B), 255–274.

[34] Zhao, H., Ding, R., Zhao, X., et al. (2017). **Graphene-based nanomaterials for drug and/or gene delivery, bioimaging, and tissue engineering.** Drug discovery today, 22(9), 1302–1317.

[35] Madni, A., Noreen, S., Maqbool, I., et al. (2018). **Graphene-based nanocomposites: synthesis and their theranostic applications.** Journal of drug targeting, 26(10), 858–883.

[35] Feng, L., Liu, Z. (2011). **Graphene in biomedicine: opportunities and challenges.** Nanomedicine, 6(2), 317–324.

[36] Cheng, J., Liu, J., Wu, B., et al. (2021). **Graphene and its Derivatives for Bone Tissue Engineering: *In Vitro* and *In Vivo* Evaluation of Graphene-Based Scaffolds, Membranes and Coatings.** Frontiers in bioengineering and biotechnology, 9, 734688.

[37] Safina, I., Bourdo, S. E., Algazali, K. M., et al. (2020). **Graphene-based 2D constructs for enhanced fibroblast support.** PloS one, 15(5), e0232670.

[38] Dash, B. S., Jose, G., Lu, Y.-J., and Chen, J.-P. (2021). **Functionalized Reduced Graphene Oxide as a Versatile Tool for Cancer Therap**y. *Int. J. Mol. Sci.* 22 (6), 2989

[39] Yao X, Yan Z, Wang X, et al. **The influence of reduced graphene oxide on stem cells: a perspective in peripheral nerve regeneration**. Regenerative Biomaterials. 2021

[40] Zhao, G., Qing, H., Huang, G. *et al*. **Reduced graphene oxide functionalized nanofibrous silk fibroin matrices for engineering excitable tissues**. *NPG Asia Mater* 10, 982–994 (2018).

[41] Lee, W. C., Lim, C. H., Shi, H., et al. (2011). **Origin of enhanced stem cell growth and differentiation on graphene and graphene oxide.** ACS nano, 5(9), 7334–7341

[42] Girão, A. F., Sousa, J., Dominguez-Bajo, A., et al. (2020). **3D Reduced Graphene Oxide Scaffolds with a Combinatorial Fibrous-Porous Architecture for Neural Tissue Engineering**. ACS Applied Materials & Interfaces.

[43] Das, S., Singh, S., Singh, V., et al. (2013). ***Oxygenated Functional Group Density on Graphene Oxide: Its Effect on Cell Toxicity.*** Particle & Particle Systems Characterization, 30(2), 148–157.

[44] Q. Zhang, X. Liu, H. Meng, S. Liu, C. Zhang. **Reduction pathway-dependent cytotoxicity of reduced graphene oxide**. Environ. Sci. Nano, 5 (6) (2018), pp. 1361-1371

[45] Tadyszak, K., Wychowaniec, J. K., & Litowczenko, J. (2018). **Biomedical Applications of Graphene-Based Structures.** Nanomaterials (Basel, Switzerland), 8(11), 944.

[46] Blanpain C., Lowry W.E., Geoghegan A., Polak L., Fuchs E. **Self-renewal, multipotency, and the existence of two cell populations within an epithelial stem cell niche** (2004) Cell, 118 (5), pp. 635-648.

[47] Kolios G, Moodley Y. **Introduction to stem cells and regenerative medicine**. Respiration. 2013;85(1):3-10.

[48] POLAK, J. M. (2006). **Stem Cells and Tissue Engineering: Past, Present, and Future**. Annals of the New York Academy of Sciences, 1068(1), 352–366

[49] Moosazadeh Moghaddam, M., Bonakdar, S., Shokrgozar, M. A., et al. (2019**). Engineered substrates with imprinted cell-like topographies induce direct differentiation of adipose-derived mesenchymal stem cells into Schwann cells.** Artificial cells, nanomedicine, and biotechnology, 47(1), 1022–1035.

[50] Ding, D.-C., Shyu, W.-C., & Lin, S.-Z. (2011). ***Mesenchymal Stem Cells.*** Cell Transplantation, 20(1), 5–14.

[51] Ffrench, B., Gasch, C., O'Leary, J.J. et al. (2014). **Developing ovarian cancer stem cell models: laying the pipeline from discovery to clinical intervention.** Mol Cancer 13**,** 262.

[52] Caplan, A. I. (1991). **Mesenchymal stem cells**. Journal of Orthopaedic Research, *9(5), 641–650.*

[53] Caplan, A. I. (2005**). Review: Mesenchymal Stem Cells: Cell–Based Reconstructive Therapy in Orthopedics**. Tissue Engineering, 11(7-8), 1198–1211.

[54] Murphy MB, Moncivais K, Caplan AI. **Mesenchymal stem cells: environmentally responsive therapeutics for regenerative medicine**. Exp Mol Med. 2013, 45-54

[55] Pittenger, M.F., Discher, D.E., Péault, B.M. et al. (2019). **Mesenchymal stem cell perspective: cell biology to clinical progress.** npj Regen Med 4, 22

[56] Tsiapalis, D.; O'Driscoll, L. **Mesenchymal Stem Cell Derived Extracellular Vesicles for Tissue Engineering and Regenerative Medicine Applications**. *Cells* 2020, *9*, 991

[57] Khosroshahi, Z., Kharaziha, M., Karimzadeh, F., & Allafchian, A. (2018). **Green reduction of graphene oxide by ascorbic acid**.

[58] Fernandez-Merino M.J., Guardia L., Paredes J.I., Villar-Rodil S., et al. (2010). **Vitamin C is an ideal substitute for hydrazine in the reduction of graphene oxide suspensions.** Journal of Physical Chemistry C, 114 (14), pp. 6426-6432.

[59] Na, Y., Song, Y. I., Kim, S. W., & Suh, S.-J. (2017). **Study on properties of eco-friendly reduction agents for the reduced graphene oxide method**. Carbon Letters, 24, 1–9

[60] **MTT Assay Protocol for Cell Viability and Proliferation.** Sigma Aldrich

[61] **Real-Time PCR (qPCR).** Stratech

[62] **How to Count Cells.** Logos Biosystems

[63] **Counting cells using a hemocytometer.** Abcam

[64] Tyler C. Moore. **Counting Cells with Hemocytometer**

[65] Klaunig, J. E., & Wang, Z. (2018). **Oxidative stress in carcinogenesis.** Current Opinion in Toxicology, 7, 116-121.

[66] Stadler, C., Rexhepaj, E., Singan, V. et al. (2013). **Immunofluorescence and fluorescent-protein tagging show high correlation for protein localization in mammalian cells.** Nat Methods 10, 315–323

[67] Kill I. R. (1996). **Localisation of the Ki-67 antigen within the nucleolus. Evidence for a fibrillarin-deficient region of the dense fibrillar component.** Journal of cell science, 109 (Pt 6), 1253–1263.

[68] Lee, W. C., Lim, C. H., Shi, H., et al. (2011). **Origin of enhanced stem cell growth and differentiation on graphene and graphene oxide.** ACS nano, *5*(9), 7334–7341.

[69] Wang, A., Pu, K., Dong, B et al. (2013). **Role of surface charge and oxidative stress in cytotoxicity and genotoxicity of graphene oxide towards human lung fibroblast cells.** Journal of Applied Toxicology, 33(10), 1156–1164.

[70] Das, S., Singh, S., Singh, V., et al. (2013). **Oxygenated functional group density on graphene oxide: its effect on cell toxicity.** Particle & Particle Systems Characterization, *30*(2), 148-157.

[71] Bak, M. J., Truong, V. L., Ko, S. Y., Nguyen, X. N., et al. (2016). **Induction of Nrf2/ARE-mediated cytoprotective genes by red ginseng oil through ASK1-MKK4/7-JNK and p38 MAPK signaling pathways in HepG2 cells**. Journal of ginseng research, 40(4), 423–430.

[72] Tang, Z., Zhao, L., Yang, Z., Liu, Z., Gu, J., Bai, B., Liu, J., Xu, J., & Yang, H. (2018). **Mechanisms of oxidative stress, apoptosis, and autophagy involved in graphene oxide nanomaterial anti-osteosarcoma effect.** International journal of nanomedicine, 13, 2907–2919.

[73] Krick, S., Eul, B. G., Hänze, J., Savai, R., Grimminger, F., Seeger, W., & Rose, F. (2005). **Role of hypoxia-inducible factor-1alpha in hypoxia-induced apoptosis of primary alveolar epithelial type II cells.** American journal of respiratory cell and molecular biology, 32(5), 395–403.

[74] Duch, M. C., Budinger, G. R., Liang, Y. T., et al. (2011). **Minimizing oxidation and stable nanoscale dispersion improves the biocompatibility of graphene in the lung.** Nano letters, 11(12), 5201–5207.

[75] Jaworski, S., Sawosz, E., Kutwin, M., et al. (2015). **In vitro and in vivo effects of graphene oxide and reduced graphene oxide on glioblastoma.** International journal of nanomedicine, 10, 1585–1596.